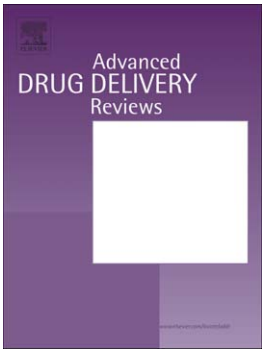

Modulating Angiogenesis with Integrin-Targeted Nanomedicines

Aroa Duro-Castano, Elena Gallon, Caitlin Decker, María J. Vicent

PII: S0169-409X(17)30064-9
DOI: doi:10.1016/j.addr.2017.05.008
Reference: ADR 13116

To appear in: *Advanced Drug Delivery Reviews*

Received date: 28 January 2017
Revised date: 12 April 2017
Accepted date: 9 May 2017

Please cite this article as: Aroa Duro-Castano, Elena Gallon, Caitlin Decker, María J. Vicent, Modulating Angiogenesis with Integrin-Targeted Nanomedicines, *Advanced Drug Delivery Reviews* (2017), doi:10.1016/j.addr.2017.05.008

Title: Modulating Angiogenesis with Integrin-Targeted Nanomedicines

[*] Dr Aroa Duro-Castano
Centro de Investigación Príncipe Felipe, Polymer Therapeutics Lab., Av. Eduardo Primo Yúfera 3, E-46012 Valencia (Spain)
Tel.: +34 963289680; Fax: +34 963289701
E-mail: aduro@cipf.es

Dr. Elena Gallon
Centro de Investigación Príncipe Felipe, Polymer Therapeutics Lab., Av. Eduardo Primo Yúfera 3, E-46012 Valencia (Spain)
Tel.: +34 963289680; Fax: +34 963289701
E-mail: egallon@cipf.es

Dr. Caitlin Decker
Centro de Investigación Príncipe Felipe, Polymer Therapeutics Lab., Av. Eduardo Primo Yúfera 3, E-46012 Valencia (Spain)
Tel.: +34 963289680; Fax: +34 963289701
E-mail: cdecker@cipf.es

[*] Dr. María J. Vicent
Centro de Investigación Príncipe Felipe, Polymer Therapeutics Lab., Av. Eduardo Primo Yúfera 3, E-46012 Valencia (Spain)
Tel.: +34 963289680; Fax: +34 963289701
E-mail: mjvicent@cipf.es

Co-Corresponding authors [*]

Abstract (150 Words)

Targeting angiogenesis-related pathologies, which include tumorigenesis and metastatic processes, has become an attractive strategy for the development of efficient guided nanomedicines. In this respect, integrins are cell-adhesion molecules involved in angiogenesis signaling pathways and are overexpressed in many angiogenic processes. Therefore, they represent specific biomarkers not only to monitor disease progression but also to rationally design targeted nanomedicines. Arginine-glycine-aspartic (RGD) containing peptides that bind to specific integrins have been widely utilized to provide

ligand-mediated targeting capabilities to small molecules, peptides, proteins, and antibodies, as well as to drug/imaging agent-containing nanomedicines, with the final aim of maximizing their therapeutic index. Within this review, we aim to cover recent and relevant examples of different integrin-assisted nanosystems including polymeric nanoconstructs, liposomes, and inorganic nanoparticles applied in drug/gene therapy as well as imaging and theranostics. We will also critically address the overall benefits of integrin-targeting.

Keywords (Angiogenesis, integrin-targeting, RGD-bearing nanomedicines, targeted drug-delivery, targeted gene delivery, integrin-assisted imaging and theranostics)

Graphical Abstract

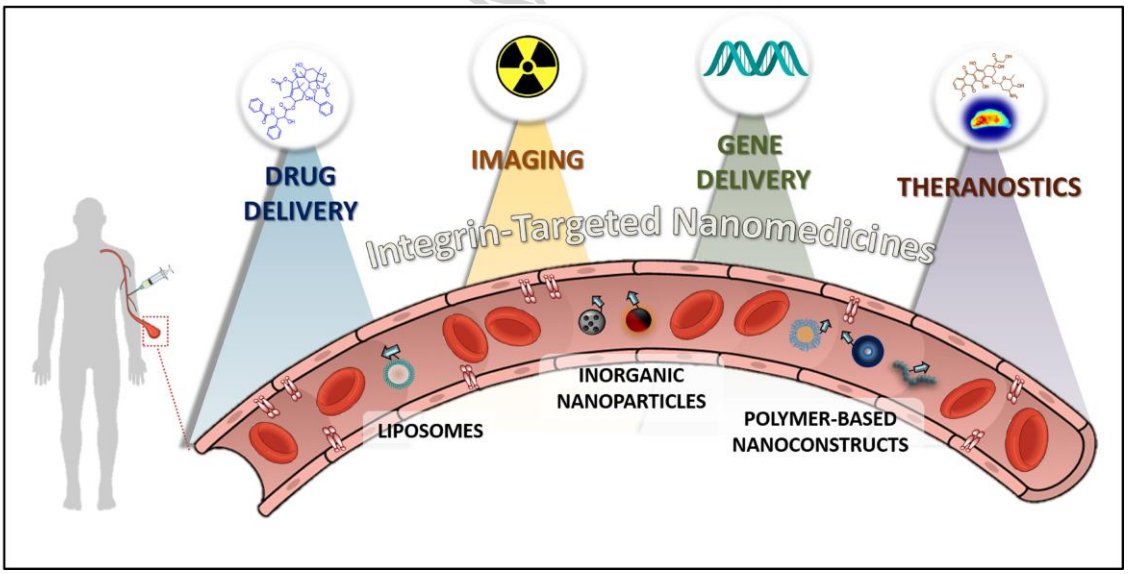

Abbreviations

(RGD)m	RGD mimetics
4-NQO	4-nitroquinoline 1-oxide
AAA	Abdominal Aortic Aneurysms
ADA	8-Amino-3,6-Dioxaoctonoic Acid
AH-GDM	Aminohexyl-Geldanamycin
ami	Amide
AP-2α	Activating Protein 2α
ARMS	Alveolar Rhabdomyosarcoma
ATO	Arsenic Trioxide
BSA	Bovine Serum Albumin
BUF	Bufalin

CAM	Cell-Adhesion Molecules
CDDP	Cisplatin
C-dots	Cornell dots
CHEMS	Cholesteryl hemisuccinate
Chol	Cholesterol
CMV	Cytomegalovirus
cRGD	Cyclic RGD
CS	Chitosan
CT	Computed Tomography
DACHPt	(1,2-diaminocylohexane) platinum(II)
DO3A	1,4,7-tris(carboxymethyl)-1,4,7,10-tetraazacyclododecane
DOTA	1,4,7,10-tetraazacyclododecane-1,4,7,10-tetraacetic acid
DOX	Doxorubicin
DSPE	1,2-distearoyl-sn-glycero-3-phosphoethanolamine
DTDE	2,2'-dithiodiethanol
DTPA	Diethylenetriaminepentaacetic acid
DTX	Docetaxel
EC	Endothelial Cells
EPI	Epirubicin
EPR	Enhanced Permeability and Retention
ESC	Esophageal Squamous Cell
FA	Folic Acid
FDA	Food and Drug Administration
FDG	Fluorodeoxyglucose
FMI	Fluorescence Molecular Imaging
FOI	Fluorescence Optical Imaging
GBM	Glioblastoma Multiforme
GDM	Geldanamycin
GEM	Gemcitabine
GNRs	Gold Nanorods
HCPT	10-Hydroxycamptothecin
HDO	1,6-Hexanediol
HFn	Human Ferritin
HSA	Human Serum Albumin
HSC	Hepatic Stellate Cells
hyd	hydrazone
i.v.	Intravenous
ICG	Indocyanine green
INP	Inorganic Nanoparticle
MMAE/F	Monomethyl Auristatin E/F
MRI	Magnetic Resonance Imaging
MSC	Mesenchymal Stem Cells
MSNPs	Mesoporous Silica Nanoparticles
MW	Molecular Weight
NIR	Near Infrared
NP	Nanoparticle

NSCLC	Non-small-cell lung carcinoma
OM	Oxymatrine
PAA	Poly(acrylic acid)
PAGE	Poly(allyl glycidyl ether)
PAI	Photoacoustic Imaging
PAMAM	Poly(amidoamine)
PC	Phosphatidylcholine
P-C	Polymer-Conjugate
PCL	Poly(ϵ-caprolactone)
PDA	Polydopamine
PDPA	Poly(2-(diisopropylamino)ethyl methacrylate)
PDT	Photodynamic therapy
PEG	Poly(ethylene glycol)
PEI	Poly(ethylenimine)
PEO	Polyethylene oxide
PEOz	Poly(2-ethyl-2-oxazoline)
PET	Positron Emission Tomography
PFD	Pirfenidone
PGA	Poly(α-L-glutamic acid)
PHPMA	Poly(N-(2-hydroxypropyl) methacrylamide)
PK	Pharmacokinetics
PLA	Poly(lactic acid)
PLK1	Polo-like kinase
PLL	Poly(L-Lysine)
PLNPs	Polymer lipid hybrid NPs
pNIPAAm	Poly(N-isopropylacrylamide)
POEGMA	Poly(oligoethylene glycol methacrylate)
Poly(CEMA)	Poly(carboxyethylmethacrylamide)
PTCA	Percutaneous Transluminal Coronary Angioplasty
PTMBPEC	Poly(2,4,6-trimethoxy benzylidenepentaerythrito carbonate)
PTT	Photothermal Therapy
PTX	Paclitaxel
PVP	Poly(vinylpyrrolidone)
QDs	Quantum Dots
QT	Quercetin
RAPA	Rapamycin
RGD	Arginine-glycine-aspartic acid
SERRS	Surface-Enhanced Resonance Raman Spectroscopy
siRNA	Small interference RNA
SLN	Sentinel Lymph Node
SP	Spermine
SPECT	Single-Photon Emission Computed Tomography
SPION	Superparamagnetic Iron Oxide Nanoparticle
TNBC	Triple Negative Breast Cancer
TPGS	D-α-tocopherol PEG-succinate
TPT	Topotecan

UCNPs	Up-conversion NPs
USPION	Ultra Small Superparamagnetic Iron Oxide Nanoparticle
VEGF	Vascular Endothelial Growth Factor
β-CD	β-cyclodextrin

1. Introduction.

1.1. Integrins and angiogenesis

Angiogenesis is the physiological process by which new blood vessels form from pre-existing vessels [1]; a process that occurs during embryonic development, growth, and wound healing. However, angiogenesis is also a fundamental process involved in the malignant transformation of tumors, tumor growth, and metastasis, as initially proposed by Folkman in 1971 [2-4]. Angiogenesis depends on, among other factors, the adhesive interaction of vascular endothelial cells (EC), and in this context, several adhesion molecules, including members of the integrin, cadherin, selectin, and immunoglobulin families are key effectors [5, 6]. Integrins represent a large family of cell-adhesion molecules (CAM) that are crucial to a wide range of cell-to-extracellular matrix and cell-to-cell interactions [7]. These cell surface receptors are heterodimeric transmembrane glycoproteins composed of two non-covalently associated α and β subunits whose combination determines ligand binding affinity and signaling properties [8]. αv integrins are overexpressed on the surface of ECs in angiogenic vessels during angiogenesis to promote their growth and survival. While the integrin extracellular domain regulates ligand binding selectivity, the cytoplasmic tail is involved in intracellular signaling pathways regulating cell adhesion, morphology, survival, migration, proliferation and invasion, by recruiting and activating specific kinases and signaling intermediates [9, 10]. For instance, integrins regulate numerous constitutively activated pathways in cancer cells, such as FAK, Erk, Src, and Rho GTPases. Integrin signaling can modulate the tumor microenvironment, while the tumor microenvironment itself also regulates tumor cells intercellular communication and the secretion of tumor-associated factors [9, 11]. Altogether, this leads to cancer proliferative effects including the induction of vascular leakiness [12], the recruitment of immune-suppressive activated immune cells such as tumor-associated macrophages (TAMs) [13], and the formation of metastatic niches via the action of disseminated cancer cells [14]. Moreover, the differential expression of integrins in tumor-derived exosomes has been described as a cell-intrinsic determinant of organ tropism of metastases. For instance, Hoshino *et al* report that a high content of exosomal integrin $\alpha_v\beta_5$ was associated to liver metastasis, whereas exosomal integrins $\alpha_6\beta_4$ and $\alpha_6\beta_1$ correlates to lung metastasis [15]. Cell-specific uptake of integrin-enriched exosomes triggers pro-

migratory and pro-inflammatory responses in the target cells, inducing the organ-specific colonization and initiation of metastasis niches.

Overall, although integrins are not oncogenic, their contribution to angiogenesis and their differential expression in disease compared to healthy conditions make integrins an excellent target to: (i) promote anti-angiogenic effects by blocking integrins actions using antagonists, (ii) block organ-specific tumor metastasis using strategies targeting exosomal integrins (iii) direct biologicals/imaging agents to tumor sites by ligand-mediated targeting or (iv) all actions combined, which may be performed via the action of nanomedicine strategies.

Among integrins, the $\alpha_v\beta_3$ integrin represents a highly specific biomarker to differentiate new and mature capillaries, allowing vascular mapping of angiogenic-related pathological situations, including tumorigenesis [16-18]. $\alpha_v\beta_3$ integrin is also one of the most studied integrins, with huge efforts expended towards the identification and production of ligands that specifically bind this receptor [19].

The widely used arginine-glycine-aspartic acid (RGD) peptide discovered by Pierschbacher and Ruoslahti [20] is considered as one of the first examples of short peptides with the ability to bind cell membrane proteins (specifically $\alpha_v\beta_3$ and $\alpha_v\beta_5$ integrins). However, linear RGD sequences were first explored due to their low affinity (nanomolar range) and their rapid degradation in biological environments. Cyclic-RGD (cRGD), which contains a conformationally constrained RGD, emerged in the hope of enhancing both selectivity and stability [21]. For instance, cyclic pentapeptides such as cRGDfK or cRGDyC, have been extensively utilized to enhance binding to certain integrins (e.g. $\alpha_5\beta_1$, $\alpha_V\beta_1$, $\alpha_V\beta_3$, and $\alpha_V\beta_5$) [22]. Additionally, the doubly cyclized peptide RGD4C (KACDCRGDCFCG) binds to $\alpha_v\beta_3$ with 20–40-fold greater avidity than linear RGD [23]. More recently, a cyclic iRGD consisting of CRGDK/RGPD, which acts as both an integrin-targeted peptide and a cell penetrating peptide, enhanced the delivery of conjugated or simply co-administered drugs or imaging agents to the tumor microenvironment and enhanced tumor penetration [24]. Figure 1 depicts examples of the most investigated RGD sequences. Alternative peptides [25], peptide mimetics [26], and antibodies [27] have also been developed to target integrins associated with the angiogenic vasculature and related proteins. Some examples are the NGR-motif binding to aminopeptidase N [28], ATWLPPR binding to VEGFR2 [29], and APRPG, which binds to a currently unidentified target [30].

Within this review, we will consider targeting agents (mostly RGD-bearing sequences) that bind integrins related to angiogenic processes involved in tumor growth and metastasis development with some notable exceptions.

1.2. Passive plus Integrin-mediated targeting - An additive effect?

Recently, nanomedicine has gained special attention in different research areas including drug and gene delivery, diagnostics and molecular imaging, as well as tissue repair and engineering [31, 32]. Clinical assessments have demonstrated that nanosystems exhibit passive targeting properties for adequately vascularized solid tumors/inflamed areas provided by the enhanced permeability and retention (EPR) effect [33-36]. However, the well accepted complexity of the tumor microenvironment and patient heterogeneity requires careful identification of EPR positive cases, and on the other hand, a search for alternative and complementary approaches [37-39]. The use of ligand-mediated targeting, in particular targeting the tumor microenvironment (including the angiogenic vasculature), has been widely considered [19, 40, 41]. Many studies have assessed conjugation of nanocarriers to integrin-targeting peptides and antibodies to improve disease site targeting and/or promote antiangiogenic effects without affecting normal tissue, therefore improving their therapeutic potential [42, 43]. Moreover, integrin-targeted nanocarriers are rapidly internalized via receptor-mediated endocytosis, employing either clathrin or caveolin-1 internalization pathways [44]. This fact is of particular relevance for the intracellular delivery of active agents and may overcome resistance mechanisms associated with cancer treatment. However, whether integrin-targeting can contribute in terms of bringing significantly higher benefits that will permit the full exploitation of this strategy in industrial development and clinical translation remains debatable. Indeed, the number of clinical studies employing integrin-targeted nanomedicines are limited due to the lack of consistent pre-clinical data [45-47].

A vast amount of studies combining passive with integrin-mediated targeting have been reported, although with different and sometimes contradictory results. For instance, Mitra and coworkers studied the tissue biodistribution of poly(N-(2-hydroxypropyl) methacrylamide) (pHPMA) of ~30 KDa molecular weight (MW) bearing integrin-specific (RGD4C) or non-specific (RGE4C) sequences and compared these polymeric conjugates with free peptides [48, 49]. *In vivo* and *ex vivo* imaging of ^{99m}Tc-labeled constructs in prostate cancer mouse models revealed significantly higher tumor accumulation for both RGD4C constructs (free or conjugated) when compared to RGE4C systems. Although both RGD4C systems demonstrated similar tumor accumulation, the free peptide exhibited higher unspecific extravasation to other organs, thereby highlighting the importance of conjugation. However, Kunjachan *et al* [50] reported contradictory results employing fluorescently labeled pHPMA of ~70 KDa MW and 10 nm in diameter bearing cRGDfK, c(CNGRC)m, or cDRfGK as a negative control. Subsequent *in vivo* and *ex vivo* imaging studies after intravenous (i.v.) administration in mice bearing highly or poorly vascularized tumors concluded that, for this particular carrier and size, passive targeting was significantly more efficient over time. Although their results may be explained by the use of a different RGD ligand, Mitra and coworkers did not observe significant differences in tumor uptake between RGDfK or RGD4C in pHPMA copolymers [51]. Nevertheless, even though all these examples used pHPMA as carrier, direct

comparison between their findings may not be applicable as they used different MW polymers, different tumor models and imaging modalities (i.e. scintigraphy methods are more quantitative/sensitive than fluorescence spectroscopy), and different contents and types of targeting moieties. In addition, within the same research group, while gold nanorods (GNR)-RGDfK conjugates did not result in significantly enhanced tumor accumulation [52], pHPMA-RGDfK conjugates displayed enhanced tumor accumulation as compared to controls in the same prostate tumor xenografts [43] altogether signifying that carrier type is important. In this particular example, the authors ascribe the lack of *in vivo* targeting of GNR-RGDfK to the presence of a negatively charged surface that likely accelerated the clearance of this system via the mononuclear phagocyte system (MPS).

These cases exemplify that ligand-mediated targeting should be evaluated on a case-by-case basis, considering both the specific conjugates and the tumor models among other factors that will influence the final biological output. In this respect, systematic studies may answer questions such as (i) which integrin-targeting sequence should be chosen for a defined biomedical application, (ii) the importance of the density and degree of exposure of the ligands, (iii) what are the binding affinities and how this can be improved using multivalency of several ligands in one carrier, (iv) what are the roles of receptor internalization, recycling, and saturation (availability of the receptor), (v) although their expression varies with tumor type and stage [53], integrins are ubiquitous receptors, which calls into question the *in vivo* specificity after i.e. systemic administration of RGD-bearing constructs, and, in a related point, (vi) what is considered an appropriate target-to-background ratio? Apart from carefully considering the intrinsic characteristics of the nanomedicine chosen (size, shape, charge…), answering these questions may allow us to better understand the real possibilities of integrin-targeting towards successful clinical use.

The present critical review tries to cover recent relevant examples of integrin-targeted systems considering polymeric nanomedicines, liposomes, and some inorganic nanoparticles, and mainly those integrins related to angiogenic processes involved in cancer and metastasis (i.e. $\alpha_v\beta_3$, $\alpha_v\beta_5$, $\alpha_v\beta_1$, or $\alpha_5\beta_1$). We hope to provide an overview of current research, describing considerations towards the design of different RGD-conjugates and their main applications. However, due to the importance of *in vivo* specificity and the role of tumor microenvironment, we will discuss only those examples with a reported *in vivo* proof of concept.

RGD peptides can also promote cell adherence to the matrix, prevent cell apoptosis, and accelerate tissue regeneration, and there are numerous examples of RGD-functionalized materials with applications in tissue engineering. However, this application is not within the scope of this review and relevant examples can be found in the literature [54].

2. Integrin-assisted drug delivery systems as antiangiogenic therapy.

The concept of targeted drug delivery brings together two important ideas; firstly, targeting to a desired body site (tissue, cell, cellular compartment), and secondly, controlled drug release to guarantee desired bioactive agent concentrations within a suitable therapeutic window. As previously mentioned, the EPR effect allows for passive targeting of nanomedicines; however, more specific mechanisms of targeting at the tissue, cellular, or even subcellular compartment level may be possible if passive targeting is combined with ligand-mediated targeting strategies to extracellular membrane receptors. Furthermore, this strategy may allow us to overcome chemoresistant mechanisms [55] and, in this regard, a large number of reports of integrin-targeted drug-delivery systems have been published in the last 30 years. Within this review, nanomedicines have been classified as polymer-based nanoconstructs including polymeric carriers (polymeric prodrugs or polymer-drug conjugates), polymeric micelles (with chemically conjugated or encapsulated drugs) and polymersomes, liposomes and liposomal formulations, and inorganic nanoparticles (INPs).

2.1. Polymer-based nanoconstructs.

2.1.1. Polymeric carriers.

Kawasaki and coworkers first performed PEGylation of RGD in the 90's with the aim of prolonging circulation time and enhancing anti-metastatic effects. PEGylation of YIGSRG with PEG3k [56] and RGD with PEG6k [57] enhanced inhibitory effects on lung metastasis of B16-BL6 melanoma mice xenografts following co-injection of the PEGylated sequences with the tumor cells [58]. Also in the 90's, Saiki *et al* performed a battery of systematic experiments to test the benefits of (RGDT)n PEGylation in the same experimental model, finding that PEGylated-RGD sequences exerted a prolonged anti-metastatic effect in all situations assessed [59]. Overall, these studies related RGD's ability to inhibit metastasis to their anti-invasive potential. Komazawa *et al* demonstrated that the poly(carboxyethylmethacrylamide-RXDS) conjugate [poly(CEMA-RXDS)], where X=G, L or l, could inhibit metastasis in different mice models [60, 61]. This conjugate efficiently diminished lung metastasis of B16-BL6 melanoma cells and liver metastasis of L5178YML25 lymphoma cells in a dose dependent manner and at concentrations where RGXS, RGXS + poly(CEMA), or poly(CEMA) did not display significant effects. Using the same model systems, RGDS-Chitin polysaccharide derivatives displayed higher anti-metastatic effects irrespective of the administration schedule (before, co-administered, or multiple dosage after inoculation of the cancerous cells) when compared to controls (RGDS, RGDS + Chitin or Chitin derivatives) [62, 63].

The potential of targeted-polymers for the treatment of tumors overexpressing $\alpha_v\beta_3$ integrin has been widely investigated. For instance, Polyak and coworkers used bifunctional PEG to conjugate $c(RGDfK)_2$

and DOX through pH-sensitive hydrazone (hyd) linkers at the terminal ends of the polymeric chain [64]. Biodistribution of the targeted polymer assessed by fluorescence imaging in a DA3 murine breast cancer model demonstrated tumor accumulation (although not significantly different) compared to an arginine-alanine-aspartic (RAD) counterpart (used as negative control). Further studies by the same group applied poly(α-L-glutamic acid) (PGA) for the design of a Paclitaxel (PTX)-bearing macromolecular drug targeted towards $\alpha_v\beta_3$ integrin using c(RGDfK)$_2$ [65]. Their polymer-drug conjugates contained 24-28% w/w RGD or RAD moiety (as negative control) with sizes of ~7 nm in diameter and led to promising *in vitro* antiangiogenic behavior, *in vivo* tumor accumulation, enhanced anti-tumor activity (1.5-fold compared to untargeted), and reduced systemic toxicity compared to free PTX.

The first report of an integrin-targeted pHPMA copolymer using linear RGD motifs was described by Wan *et al* [66], with the final conjugate demonstrating enhanced *in vitro* uptake by ECV304 endothelial cells as well as altered conjugate intracellular localization. Following this first study, Ray and coworkers synthesized a RGDfk-pHPMA-Docetaxel (DTX) conjugate of 3 nm in diameter and a RGD content of ~5% w/w [67]. The authors compared ligand-mediated targeting with this conjugate *vs* passive targeting of copolymers with high MW and 7.6 nm in size. They found that a single treatment dose of either conjugate in a DU145 prostate cancer xenograft model was sufficient for tumor regression. The same group also reported that RGDfK-pHPMA-GFLG-aminohexyl-geldanamycin (AH-GDM) containing 6.1 RGD units/polymer exhibited a 2-fold greater tolerated dose than free AH-GDM in the same animal model [68]. Additionally, biodistribution studies using a ^{125}I radiolabeled version of the conjugates revealed significantly higher tumor accumulation (up to ~3 fold at 12 hours) for the targeted compared to non-targeted polymer [69]. Finally, the authors obtained *in vivo* proof of efficacy of this conjugate by demonstrating anti-tumorigenic and antiangiogenic activity in the same DU145 prostate cancer xenograft model [70], thus demonstrating that an HPMA carrier bearing cRGD motifs offered a more promising approach than linear counterparts [43].

To the best of our knowledge, Shukla *et al* reported the first integrin-targeted poly(amidoamine), or PAMAM, dendrimer [71]. Generation 5 (G5) PAMAM dendrimers bearing RGD4C (2-3 peptide/dendrimer) exhibited efficient *in vitro* targeting to $\alpha_v\beta_3$-expressing cells. Following this study, the group of Jiang extensively studied PEG-PAMAM-cys-aconityl-DOX (PPCD) dendrimers as an antitumor therapy [72, 73]. As an additional step, the authors linked 16.8 cRGDyC units per PAMAM through a PEG linker leading to 17 nm conjugates. When evaluated *in vivo* in a murine B16 melanoma tumor model [74] and in orthotopic murine model of C6 glioma [75], RGD-PPCD demonstrated a 1.46-fold increase in tumor accumulation compared to PPCD and permitted significantly increased survival rates (>3-fold). Another study substituted the cRGDyC moiety for iRGD and found that the iRGD versions

of the system (conjugated or co-administrated) exhibited better tumor penetration and accumulation and this translated to higher survival rates *in vivo* [76]. Even given this success, further studies explored the added potential of RGD-PPCD loaded onto poly(lactic-co-glycolic acid)-poly(lactic acid) (PLGA-PLA) implants for long-term intratumoral release [77]. These implants led to better intratumoral drug accumulation (~4-fold compared to free DOX implants) and consequently, they exhibited enhanced antitumor activity in C6 glioma xenografts (~2- and ~1.3-fold lower tumor volume when compare to DOX and untargeted implants, respectively). Finally, the same group used mesenchymal stem cells (MSCs) loaded with RGD-PPCD to provide tumor tropic delivery and to improve conjugate tumor penetrability [78]. In this case, MSCs provided the tumor-targeting characteristics, as MSC-PPCD equipped with RGD exhibited similar antitumor effects, similar tumor penetrability, and increased survival time (41-45 days) compared to MSC-PPCD without RGD when injected intracranially in their C6 glioma mice model.

Very recently, Xu *et al* developed a novel redox-responsive polymeric prodrug based on polycondensation of 10-hydroxycamptothecin (HCPT) with 2,2'-dithiodiethanol (DTDE) or 1,6-hexanediol (HDO) [79]. The resulting polymer also incorporated a PEG block and GGRGD tail yielding nanoconstructs of <70 nm in diameter. This mode of targeting allowed for a two-fold greater tumor accumulation in HepG2 tumor-bearing mice compared to an untargeted nanoconstruct. Moreover, the targeted system displayed comparable antitumor effects to free HCPT, but with lower side effects and an increased survival rate (Figure 2).

2.1.2. Polymersomes

Polymersomes, polymeric vesicles formed by self-assembly of block-copolymers, have recently garnered attention as promising drug and gene delivery vectors [80]. Yang and coworkers evaluated a series of cGRGDSPK-polymersomes of PEG-*block*-P(ϵ-caprolactone) (PEG-PCL) of 95 nm diameter loaded with Oxymatrine (OM) as a therapy for liver fibrosis [81]. The loaded polymersomes exhibited improved antifibrotic activity in hepatic stellate cells (HSCs) and a bile duct-ligated rat model when compared to the untargeted system and the free drug. In another example, Simón-Gracia *et al* developed iRGD-conjugated pH sensitive polymersomes of poly(oligoethylene glycol methacrylate)-poly(2-(diisopropylamino)ethyl methacrylate) (POEGMA-PDPA) loaded with PTX to treat peritoneal carcinomatosis [82]. The 214 nm diameter polymersomes boasted a peptide loading of 1.6 x 10^3 units/polymersome. Results obtained in mice bearing peritoneal tumors from gastric (MKN-45P) or colon (CT26) origin demonstrated higher tumor-selective accumulation and penetration. Furthermore, the authors of the study observed an improved inhibition of both tumor growth (~1.4-fold) and local dissemination (1.7-fold) when compared to untargeted conjugates.

Finally, Chen *et al* constructed DOX and PTX incorporated 23 nm core-shell polymersomes from a cRGDyK-Pluronic F127 conjugate for angiogenic and blood-brain-barrier (BBB) targeting [83]. When tested in a U87MG brain glioma mice model, the RGD-system demonstrated greater intracranial tumor accumulation (up to 1.45-fold) and increased survival rate (8 days when compared to untargeted, and 16 days when compared to control) [84]. Similar targeting benefits were also obtained when tested in MDR human squamous carcinoma (KBv) bearing mice [85].

2.1.3. Polymeric micelles

The application of integrin-targeted polymeric micelles represents a popular strategy given the large number of studies devoted to their development. For example, Hu *et al* prepared nanosized RGD4C-PLA-polyethylene oxide (PEO) micelles of ~128 nm loaded with PTX [86]. ^{125}I-labeled targeted RGD4C-PLA-PEO micelles demonstrated significantly higher tumor uptake (3.3-fold increase) when compared to untargeted micelles and PTX-loaded targeted micelles exhibited enhanced antitumor activity with an almost complete reduction in tumor size in MDA-MB-435 tumor bearing mice. In another example, Gao *et al* prepared cRGDyK-conjugated pH-sensitive poly(2-ethyl-2-oxazoline)-PLA (PEOz-PLA)/PTX micelles for prostate cancer treatment [87]. Micelles had a diameter of 28 nm, displayed appropriate integrin targeting *in vitro* and, when assayed in a PC-3 tumor bearing mice xenograft model, exhibited significantly higher antitumor activity compared to untargeted micelles or Taxol.

In another study, Zhan and coworkers synthesized cRGDyK-PEG-PLA/PTX micelles with PTX and ~35 nm diameter [88] and studied their activity in U87MG glioblastoma bearing mice. Their findings demonstrated that targeted micelles effectively accumulated in tumor tissue and, when loaded with PTX, they exhibited enhanced antitumor effects in terms of tumor volume reduction (7-fold decrease compared to control) and mean survival of the animals (48 days *vs* 41.5 of untargeted and 34 of saline). Following this study, Li *et al* employed similar cRGDyK-PEG-PLA micelles to encapsulate DTX, creating spherical constructs with a diameter of ~ 100 nm [89]. As for their PTX analogues, targeted-DTX micelles significantly inhibited tumor growth in U87MG glioblastoma bearing mice (~5 times less tumor volume compared to control and 2 times when compared to untargeted micelles). Similarly, RGD-PEG-PLA loaded with curcumin (4.7 %) by Zhao *et al* led to the formation of spherical micelles of ~20 nm [90]. However, targeting via RGD only permitted a small increase in antitumor activity (as measured by tumor growth) when compared to untargeted micelles in B16 tumor-bearing mice.

Subsequently, Xiong *et al* developed PEO-PCL micelles with RGD4C (10% mol) [91] with DOX conjugated into the micellar core using cleavable hydrazone (hyd) bonds or stable amides. These systems of 60-90 nm size were tested both *in vitro* and *in vivo* models using two different strains of the MDA-435 model

(DOX-sensitive LCC6^{WT} or DOX-resistant LCC6^{MDR}). RGD conjugation increased cellular uptake and tumor accumulation in all cases and, interestingly, hyd-DOX systems demonstrated nuclear accumulation and increased anti-tumor activity in the LCC6^{WT} models, whereas ami-DOX micelles displayed mitochondrial accumulation and better results in the LCC6^{MDR} models.

The Kataoka group developed 30 nm PEG-PGA micelles incorporating (1,2-diaminocylohexane) platinum(II) (DACHPt) and conjugated different loadings of cRGDfK onto the micelle surface [92, 93]. When tested in a U87MG human glioblastoma orthotopic mouse model, 20% mol cRGDfK targeted micelles demonstrated higher selectivity, faster accumulation in tumor tissue (2.2-fold at 4 h vs 20% cRAD-micelles), and provided the highest growth inhibitory effect (about 6-fold more compared to cRAD-micelles) [93]. A second study tested these micelles against lymph node metastasis in a syngeneic melanoma model. While targeted and untargeted micelles exhibited similar effects in the primary tumors, the targeted micelles demonstrated an enhanced anti-metastatic effect [92] in agreement with above-mentioned examples [60-63]. Song *et al* also developed PEG-PGA micelles [94] via cisplatin (CDDP)chelation using PGA side-chain carboxylic groups (COOH). Co-administration of micelles of 5-26 nm with iRGD in an *in vivo* non-small-cell lung carcinoma (NSCLC) xenograft model (A549) led to prolonged circulation time, elevated anti-tumor activity, vastly reduced toxicity, and prolonged survival times. However, co-administration with iRGD did not improve passive targeting.

Guan and coworkers exploited cRGDfK in various micellar systems to achieve enhanced tumor targeting [95-97]. Integrin-targeted hybrid micelles of 18 to 60 nm were constructed in aqueous media by co-assembling 20% cRGDfK-PEG-PLA and 80% epirubicin (EPI) conjugated to mPEG-poly(allyl glycidyl ether) (mPEG-PAGE-EPI). In this case, EPI was conjugated via pH sensitive carbamate or hydrazone linkers. These nanoconstructs displayed enhanced antitumor activity when compared to free EPI in B16F10 mice xenograft, with the hyd-EPI micelles (untargeted and targeted) displaying the greatest activity [97].

Pan *et al* synthesized 33 nm spherical micelles using random copolymers of P(OEGMA-co-poly(methacryloyloxy)ethyl)thio)propanoic acid), P(OEGMA-co-BSMA) [98] and introduced the anticancer drug bufalin (BUF) via ester bonding and cRGDyK through an aminolysis reaction. These systems exhibited increased specific accumulation and prolonged retention time in tumors and, as a result, the study observed greater antitumor activity in terms of an increase in apoptosis and the inhibition of angiogenesis and tumor growth in animals treated with targeted micelles (1.8-fold and 3-fold tumor inhibition compared to untargeted or free BUF).

2.1.4. Polymeric nanoparticles (NPs)

Regarding polymeric nanoparticles (NPs), Temming and coworkers developed cRGDf(ε-S-acetylthioacetyl)K conjugates of human serum albumin (HSA), with and without a PEG spacer, bearing the antitubulin agent monomethyl auristatin E [99] or F [100] (MMAE, MMAF). These RGD-(PEG)-MMAE/F-HSA NPs demonstrated selective targeting of integrin-expressing cells *in vivo* in C26 carcinoma bearing mice, although the study did not perform adequate quantification.

In another study, Ji *et al* recently reported c(RGDyK)C-bovine serum albumin (BSA) crosslinked NPs of 130 nm with encapsulated Gemcitabine (GEM) as a potential treatment for pancreatic cancer [101]. Treatment of BxPC-3 pancreatic cancer xenografts with RGD-BSA/GEM NPs displayed significantly better results compared to the control group (6-fold tumor reduction) and to treatments with GEM or BSA/GEM. These results are of particular importance since pancreatic cancer treatment with nanoconstructs is specially challenging due to the lower vascular density of these types of tumors making them poorly accessible by EPR-mediated tumor targeting strategies [102]. Thus, ligand-mediated targeting strategies may represent a suitable approach, although endothelium targeting in poorly vascularized tumors can be counterintuitive could facilitate at least organ tropism and after adequate drug release within tumor microenvironment significantly enhance nanomedicine therapeutic output.

Graf *et al* developed cRGDfK bearing NPs of PLGA-PEG of 120 nm diameter containing an encapsulated cisplatin Pt(IV) analogue [103]. *In vivo* performance in a MCF7MFP1 breast cancer xenograft model demonstrated that both CDDP and the cRGD-PLGA-PEG/CDDP NPs exhibited similar tumor growth inhibition (~60%). However, the application of NPs improved safety and caused lower levels of nephrotoxicity. In another study, Zhu *et al* developed PTX-loaded PCL-poly(vinylpyrrolidone) (PCL-PVP) NPs modified with 10% iRGD on the NP surface [104]. These systems, of 40-60 nm in size, revealed enhanced tumor accumulation (1.5-2.7 fold more than untargeted) and enhanced penetration, resulting in greater tumor growth inhibition (58- 68% smaller tumors than Taxol® treated group) and life span prolongation in mice bearing H22 hepatic tumors. Zhang *et al* next developed EPI loaded polysaccharide Inulin-ibuprofen-cRGDfK self-assembled NPs of ~150 nm [105]. *In vivo* antitumor activity studies in hepatic H22 tumor-bearing mice demonstrated a greater inhibition of tumor volume when compared to free EPI (2.09-fold) or untargeted NPs (1.29-fold).

Alternatively, Qiu *et al* developed stimuli-responsive NPs based on PEG-poly(2,4,6-trimethoxy benzylidenepentaerythrito carbonate) (PEG-PTMBPEC) block copolymer [106]. These NPs were used to encapsulate DOX and were further modified on the surface with cRGDyK (up to 20% mol) leading to homogeneous spherical systems of 180 nm. *In vivo* studies demonstrated greater tumor inhibition by the targeted NPs when compared to untargeted NPs (2.2-fold lower final tumor weight) and to saline (3.7-fold lower final tumor weight) alongside significantly reduced systemic toxicity.

Lastly, Guo *et al* employed TPGS-SS-PLA NPs with 1 mol% cRGDfC moieties attached to the surface to load PTX [107]. These cRGD-NPs of about 130 nm displayed a prolonged half-life and significantly greater tumor growth inhibition capacity (~2-fold) as compared to untargeted NPs or Taxol® in mouse sarcoma S180- and B16F10-tumor bearing mice.

2.2. Liposomes and liposomal formulations.

Liposomes have also been extensively used in targeted drug delivery [108]. Liposome-assisted delivery to new and abnormal vasculature has been mainly approached using long circulating liposomes (LCL) with PEG as a stealth moiety. For instance, Schiffelers *et al* developed cRGDf(ε-S-ac-thioac)K-PEG-DSPE LCL loaded with DOX and a total of ~300 peptides per liposome [109]. Although RGD-bearing LCLs did not display a significantly different accumulation in tumors compared to its untargeted counterpart, the study found a 2.5-fold greater tumor reduction when testing these targeted liposomes in C26 DOX-resistant carcinoma bearing mice.

In a another study, Xiong *et al* prepared DOX loaded liposomes from phosphatidylcholine (PC) derivatives, DSPE, and PEG and decorated each formulation with an RGD mimetic (RGD_m) [110] or an RGD tripeptide [111] yielding stabilized liposomes of ~120 nm. In both cases, treatment of B-16 melanoma bearing mice led to enhanced suppression of tumor growth (>1.5-fold) compared to control untargeted formulations. Using similar liposomal formulations including cholesterol (Chol), the authors developed RDG(5% mol)-bearing PTX loaded systems of ~120 nm [112]. Treatment of a SKOV-3 human ovarian cancer mouse model with these constructs permitted a 1.4-fold higher level of tumor growth inhibition compared to liposomes lacking the targeting agent. The same research group [113, 114] also constructed analogue DOX-loaded liposomes linked with the Ac-PHSCN-NH_2 (ATN-161) $\alpha_5\beta_1$ ligand and antagonist [115]. Antitumor efficacy studies of ~100 nm targeted liposomes carried out in mice bearing B16F10 tumors revealed tumor growth inhibition at 3-fold and 6-fold higher levels compared to control liposomes and free DOX respectively, with extended survival times and reduced cardiotoxicity. The same authors also linked the integrin-targeting cyclic peptide c(CDGF(3,5-DiF)G-Hyp-NC [116, 117] to similar DOX-carrying liposomes of 100 nm [118]. Combined therapy of these targeted liposomes with PEG-PCL micelles carrying rapamycin (RAPA) inhibited tumor growth in a MDA-MB-231 breast cancer mice model to a level ~2-fold and 3.5-fold greater than single targeted-liposomes/DOX and Micelles/RAPA, respectively.

Cao and coworkers obtained comparable liposomes of ~100 nm loaded with PTX and surface decorated with cRGDyk [119] and these targeted liposomes reduced tumor volume by 1.2 fold in a PC-3 tumor xenograft model as compared to the untargeted formulation. Likewise, Scherzinger-Laude *et al* loaded

cRGDfC-liposomes with the microtubule stabilizer and antiangiogenic drug patupilone (EPO906) yielding nanoconstructs of 100 nm [120]. In this case, i.v. administration to Kelly neuroblastoma and RH30-rhabdomyosarcoma bearing mice revealed a potent antitumor effect for both targeted and untargeted liposomes with complete tumor reduction. Also using similar liposomal formulations, Shi *et al* developed pH-sensitive constructs loaded with PTX and decorated with a tandem peptide (TR - cRGDfKC and cell penetrating TH peptide [121]) for the treatment of aggressive glioma. Targeted liposomes of 110 nm were administered *in vivo* in glioma-bearing mice, and near-infrared imaging and antitumoral activity studies found high levels of tumor accumulation and an increase in survival time of mice from 30.5 (PEG-liposomes) to 45 days (TR-liposomes).

Ji *et al* further modified smart liposomes carrying GEM and surface decorated with Ac-CRGDS (5% w/w) via surface conjugation with the polymer conjugate β-cyclodextrin (β-CD)-Pirfenidone (PFD) through an enzyme responsive linker as a treatment for pancreatic cancers [122]. Completed liposomes displayed sizes of ~130 nm and *in vivo* studies performed in mice bearing PSCs and Panc-1 co-implanted tumors indicated to a 3-fold increase in tumor growth inhibition compared to the control formulation.

An a separate set of studies, the Cui group prepared liposomal preparations from fatty alcohols and surface modified liposomes with 5% mol RGDF [123]. Biodistribution and PK studies of a DOX loaded construct in a mouse model of sarcoma demonstrated a 4.6 fold higher targeting efficiency compared to DOX alone and 2.1 fold higher than control liposomes. In their next study, the group loaded liposomes with DTX and screened the effect of fatty alcohol chain length and the addition of the F or V amino acids to RGD peptide to the targeting efficiency of the system [124]. *In vitro* and *in vivo* data demonstrated the essential nature of 5% mol tripeptide sequence RGD, but neither the addition of a fourth amino acid nor a change in chain length improved tumor targeting. In general, all RGD-bearing liposomes induced tumor inhibition by around 70% compared to the 30% of conventional liposomes when injected in S_{180} sarcoma bearing mice.

Next, Chang *et al* developed and administered RGD-targeted pH-sensitive liposomes of 130 nm from cholesteryl hemisuccinate (CHEMS) loaded with DTX [125] to MCF7 breast cancer harboring mice. The authors claim that this formulation achieved higher tumor accumulation compared to an untargeted control, although the study lacked proper quantification. Zhang and coworkers synthesized and tested pH sensitive cRGDfKC(6% mol)-PTX-liposomes of 146 nm decorated with the cell penetrating peptide [D]-H_6L_9 in C26 tumor-bearing mice by [126]. In this case, the targeted liposomes displayed a 2-fold greater reduction in tumor volume as compared to treatment with PEG-liposomes.

Liang *et al* constructed immunoliposomes with an Integrin β_6-targeting monoclonal antibody (E7P6) attached to the surface [127]. Integrin β_6 is commonly associated with invasion, metastasis, and chemotherapeutic resistance in colon cancers. Immunoliposomes of 405 nm loaded with 5-fluorouracil (5-FU) were i.v. injected in mice bearing HT-29 and SW480b6 human colon cancer xenografts and this permitted a tumor volume suppression ~3-fold higher compared to 5-FU liposomes without E7P6.

Very recently, Bao and coworkers conjugated DOX to d-α-tocopherol PEG-succinate (TPGS) via Schiff base bonding [128] and formulated conjugate with cRGD-conjugated-PEGylated lipid 1,2-distearoyl-sn-glycero-3-phosphoethanolamine (cRGDfC-DSPE-PEG) to form hybrid lipid micelles of ~150 nm diameter. When tested *in vivo* in different aggressive tumor mice models (MCF-7/ADR resistant breast cancer, B16F10 melanoma, and H22 hepatocellular carcinoma), the RGD-bearing micelles displayed enhanced inhibition of tumor growth and metastasis.

Additionally, Saraf *et al* prepared RGD-micelles from peptide amphiphiles based on C_{16} or C_{18} fatty acids with 1-5 units of 8-amino-3,6-dioxaoctonoic acid (ADA) to which RGD moieties (linear or cyclic for comparison) were conjugated [129, 130]. For $C_{18}(ADA)_5$-RGD(linear or cyclic)/PTX micelles of 140 nm, *in vivo* efficacy studies conducted in melanoma mouse xenograft [129] concluded that cRGD lipid micelles displayed better targeting efficacy but less antitumor activity compared to linear RGD micelles. The study suggested that these characteristics may be a consequence of lower loading capacity and stability.

Finally, Shi *et al* developed RGD conjugated DSPE-PEG/lecithin/PLGA polymer lipid hybrid NPs (PLNs) loaded with DTX for the targeted treatment of glioblastoma multiforme (GBM) [131]. These RGD-targeted constructs of 110 nm exhibited the greatest brain accumulation and antitumor efficacy (in terms of survival time) of GBM-bearing rats (1.43-fold higher compared to untargeted and 3.55-fold higher compare to saline). Agrawal and coworkers employed the same PLNs to encapsulate cRGDfK-PTX and conjugate Folic Acid (FA) to the surface [132] in a dual targeting approach. Their potential was demonstrated *in vivo* in a T98G human glioblastoma xenograft mouse model, where the complete dual-targeted system showed the greatest median survival of 42 days. This value was 1.1-fold higher compared to NPs lacking RGD, 3-fold higher when compared to free PTX, and 3.5-fold higher compared to a saline only control.

2.3. Inorganic Nanoparticles.

Although the star application of integrin-targeted inorganic nanoparticles (INPs) is imaging and theranostics (with the unique example of RGD-targeting so far in the clinics [45, 46]), several examples of applications in drug delivery also exist. For instance, the functionalization of mesoporous silica nanoparticles (MSNPs) with targeting peptides for drug delivery has recently been extensively reviewed

[133-135]. In one example, Murugan *et al* loaded both topotecan (TPT) and quercetin (QT) in cRGD-bearing poly(acrylic acid) (PAA)/chitosan (CS) modified MSNPs of 65–75 nm [136]. When these systems were tested in mice bearing MDA-MB-231 breast carcinomas, targeted MSNPs decreased tumor volume by 85% compared to the untreated control. This result is significantly better than untargeted MSNPs (70% decrease) and free drugs (41% for TPT, 38% for QT). Similarly Xiao and coworkers loaded DOX into ~130 nm MSNPs and added the RGD peptide c(RGDWWW)$_2$KC as a redox sensitive gate-keeper and therapeutic agent aiming for synergism [137]. Encouragingly, both untargeted and targeted MSNs reduced tumor volume in a murine H22 hepatic tumor xenograft model by a level 2-fold greater than free DOX.

Zhao and coworkers encapsulated gold nanorods (GNRs) within MSNPs and covalently modified the surface with cRGDfC, yielding ~80 nm cRGD-MSNs/GNR for megavoltage therapy of triple negative breast cancer (TNBC) [138]. Constructs injected in TNBC mice 24 hours prior to a 10 Gy irradiation with cRGD-MSNs/GNR mediated significantly greater decreases in tumor growth (1.9-fold and 2.3-fold greater than untargeted and x-ray irradiation only, respectively). In another example of TNBC treatment with MSNPs, Wu and coworkers encapsulated arsenic trioxide (ATO) within 100 nm MSNPs modified with 0.20 mmol/g cRGDfK [139]. *In vivo* studies conducted in mice bearing MDA-MB-231 breast tumors resulted in a ~2-fold greater loss in tumor weight in animals treated with RGD-MSNPs/ATO than animals in the untargeted treatment group. Finally, Yeh and coworkers developed PEG-coated FITC-GARGDLASLC-conjugated GNRs to enhance tumor targeting for radiotherapy [140]. Twelve hours after injection in mice harboring HSC3 oral squamous carcinoma, the authors observed high tumor-to-other tissues ratios of accumulation, although this system was not compared with its untargeted counterpart.

Summarizing the data described so far in Section 2, and considering all the examples of integrin-assisted drug delivery systems from a critical point of view, we can draw several conclusions. The majority of the cases provided in this section (64 %) (See Table 1) employed stabilized and cyclic versions of peptides with higher described integrin-avidity *vs* their linear analogues. However, due to the differences in the nanoconstructs employed (size, z-potential, etc.) and the large discrepancy concerning the number of peptide units included, general conclusions about ligand density and multivalency approaches cannot be drawn. It is clear though that, most positive *in vitro* results translated to positive *in vivo* results; higher tumor accumulations and/or antitumor and anti-metastatic effects (84% of the cases discussed). Nonetheless, around half of the reviewed targeted examples only outperformed untargeted conjugates by less than 1.5-fold, with many untargeted conjugates already exhibiting excellent anti-tumor characteristics. The preclinical model selected to perform the experiments is also of crucial importance

as, in many cases, xenografts do not perfectly reflect the real vascularization encountered in a native human tumor and, therefore, the results obtained may not be entirely reliable [141]. Additionally, only a few cases employed adequate *in vivo* blocking studies using co-injection of RGD to assess real *in vivo* specific integrin-targeting. Whether these small but significant improvements should be promoted to industrial development/clinical application may only be valued in terms of feasibility and increased costs. However, on a more encouraging note, 50% of the cases demonstrated that the appropriate use of RGD sequences may increase anti-metastatic potential and enhance antitumor efficacy of polymer-based drug delivery systems by increasing tumor uptake and providing synergistic effects as anti-metastatic agents, mostly in those cases where passive targeting by the EPR effect already has a positive role.

3. Integrin-assisted gene therapy approaches.

Gene therapy has been postulated as strategy to treat diseases/disorders associated with genetic mutations through the targeted delivery of therapeutic oligonucleotides. The rise of non-viral vectors, whose clinical progress has accelerated in recent years [142], has overcome many limitations of classical viral vectors. These include a limited capacity to carry genetic materials, immunogenicity, cytotoxicity, the possibility of insertional mutagenesis, and manufacturing-related problems. However, one of the main criticism of non-viral vectors is the lack of specific cell targeting. Ligand-mediated targeting strategies emerge here as a possible alternative.

3.1. Polymer-based nanoconstructs.

Numerous examples of integrin-targeted gene delivery systems have been reported, mainly employing positively charged polymers to form stable polyplexes or micellar and nanoparticulated systems. For instance, Aoki and coworkers synthesized an RGD-based motif conjugated to a histidylated oligolysine CRGDCF(K[H-]KKK)$_6$ or cRGD-hK that complexed with cytomegalovirus (CMV) promoter-driven luciferase (Luc) expression plasmids [143]. Luciferase activity detected in two different mice tumor models (PLC hepatoma and MIAPaCa-2 pancreatic) after *i.v*. administration of the complexes was significantly higher in tumors compared to other organs. However, the study also observed significant liver accumulation and, furthermore, they did not perform comparisons with untargeted complexes.

In another recent example, Cao *et al* employed RGD-G1-PAMAM with 2.6% cRGDfC to complex and deliver a plasmid vector carrying a *VEGF* gene construct (pVEGF165) in order to induce angiogenesis and prevent restenosis related to percutaneous transluminal coronary angioplasty (PTCA) performed following myocardial infarction [144]. The nanocomplex exhibited a particle size of 80-160 nm with a positive z-potential (3-20 mV). *In vivo* experiments in a rabbit model of carotid artery injury determined

that the RGD-containing complex provided the highest levels of recombinant plasmid-derived VEGF protein (1.6-fold more compared to untargeted and 2.3-fold more compared to saline), and hence, performed better in reducing PTCA-associated pathological hallmarks.

Similarly, Schiffelers and coworkers employed cRGD-PEG-PEI containing 40 cACRGDMFGCA units/PEI to form stable complexes of 100 nm with an siRNA targeting vascular endothelial growth factor receptor-2 (VEGFR2) in order to inhibit tumor angiogenesis and, therefore, tumor growth [145]. I.v. administration of this system to N2A tumor-bearing mice led to selective tumor uptake, ~90% gene silencing efficiency *in vivo*, and inhibition of angiogenesis and tumor growth. Kim *et al* also followed a VEGF silencing strategy via the application of the soluble fragment of the Flt-1 VEGF receptor (sFlt-1) to block VEGF receptor binding [146]. This strategy also employed cRGD-PEG-PEI with 1.3 cACRGDMFGCA units/PEI to form complexes of 100-200 nm and a positive z-potential (+32 mV) with a pCMV-sFlt-1 plasmid. Following i.v. administration of the targeted complex to CT-26 colon adenocarcinoma xenograft mice model [147], the authors observed a 3-fold reduction in tumor growth. In a later study, the same carrier was used to deliver siRNA against VEGFR1, forming complexes of ~160 nm and slightly positive z-potential. When tested in the same animal model, the study observed a 1.7-fold greater tumor growth inhibition for the integrin-assisted system [148].

Very recently, Wang and coworkers encapsulated an AP-2α (activating protein 2α) expression plasmid (pCMV6-AP-2α) using an integrin-targeted P123 Pluronic block copolymers [149], creating constructs (targeted and non-targeted) with a particle size of ~20 nm in diameter and 1% w/w of cRGDfK peptide. AP-2α regulates cell function by targeting related cancer genes (by inhibiting the expression of Bcl-2 protein and stimulating the Bax/Cytochrome/Apaf1/caspase-9 signaling pathways, among other actions) and when tested *in vivo* in a primary gastric tumor animal model, the targeted conjugate reduced tumor size and weight to a greater degree than the untargeted conjugate (68.4 % reduction from control, 4-fold greater reduction than untargeted).

Garg and coworkers employed PEO-*b*-poly(ϵ-caprolactone-grafted-spermine) (PEO-*b*-P(CL-g-SP)) micelles for the targeted delivery of MCL-1 siRNA, an antiapoptotic member of Bcl-2 family [150]. The introduction of cholesterol units in the inner core, to increase transfection efficiency, and RGD4C peptide on the shell yielded complexes of 60-70 nm diameter and slightly negative z-potential. When tested *in vivo*, RGD4C presence significantly improved transfection efficiency (~40 % silencing *in vivo*) although cholesterol modifications had no effect.

Scheinman and coworkers developed RGD-PLGA NPs for the delivery of STAT1 siRNA, leading to the assembly of spherical objects of ~250 nm size and neutral z-potential [151]. When tested in a mouse

model of rheumatoid arthritis, NPs boosted tissue uptake (10- to 200-fold more in injured paw), reduced STAT1 mRNA levels, and these improvements correlated to disease regression. In a similar study, Shen *et al* produced iRGD-TPGS/Pluronic P85-PEI NPs used in the co-delivery of PTX and Survivin short hairpin RNA (shRNA) [152]. These NPs displayed a stable, small particle size (141−160 nm) and positive z-potential (+30 mV) with a PTX loading of 1.88 %. The targeted systems provided significantly greater *in vivo* results in terms of PTX and shRNA accumulation in tumor tissue, downregulation of Survivin expression (~80 % downregulation), and elevated *in vivo* antitumor activity. Overall, tumors in targeted NP-treated animals displayed a tumor volume only 12.7 % of free PTX group, a level 2-3-fold less than that found in the untargeted NP group.

3.2. Liposomes and liposomal formulations

Due to the negatively-charged nature of oligonucleotides, cationic lipids that complex or aid in oligonucleotide conjugation are usually preferred for gene delivery purposes [153]. For instance, Hood and coworkers used cationic lipid-based NPs to conjugate a mutant *Raf* gene, which blocks endothelial signaling and angiogenesis [154], and introduced a small integrin synthetic antagonist to provide α_v3_β targeting. Inoculation of these lipid nanoparticles in mice bearing M21-L melanomas led to rapid tumor regression compared to controls with no evidence of tumor presence and a high suppression of blood vessel density 6 days after treatment.

In another study, Majumder and coworkers applied RGDK-PEG-lipopeptides [155, 156] together with cholesterol and cationic lipid amphiphiles to encapsulate CDC20 siRNA in 160-180 nm liposomes of slightly positive z-potential. The cell cycle regulator CDC20 is essential for cell division in many cancers [157], and treatment of mice bearing aggressive melanomas with these targeted liposomes mediated an almost complete tumor reduction with ~10-fold greater tumor growth inhibition compared to untargeted liposomes (Figure 3).

For Alveolar rhabdomyosarcoma (ARMS) treatment, Rengaswamy *et al* developed RGD(15% mol)-Lipid–Protamine-siRNA (LPR) NPs with a size of 222 nm and a positive z-potential [158]. ARMS are aggressive soft tumors characterized by specific fusion transcripts such as PAX3-FOXO1 (P3F) [159]. Encapsulation of P3F-siRNA in this liposomal formulation permitted a gene knockdown of 63.5% *in vitro*. However, the *in vivo* experimental design conducted in ARMS Rh30 mice xenograft only allowed them to conclude that the targeted strategy delayed tumor initiation, as this strategy failed to inhibit the growth of already established tumors.

A separate study employed the pH sensitive cationic lipid YSK05 [160] with further lipid components to yield cRGDfK-PEGylated liposomes of 100 nm to encapsulate VEGFR2 siRNA [161]. *In vivo* antitumoral

activity performed in OS-RC-2-bearing mice revealed that targeted-liposomes caused 2-fold higher inhibition of tumor growth compared to a control targeted siRNA against the Luciferase gene. However, this study lacks a comparison with an untargeted liposome to fully understand the benefits of targeting.

Adil *et al* employed $\alpha_5\beta_1$ integrin targeted liposomes using 5% mol PR_b peptide [25, 26] to load branched PEI/pDNA complexes of a luciferase transgene plasmid [162] and assessed therapeutic potential of 280 nm formulations in a CT26 colon carcinoma model. While i.v. injected PR_b functionalized liposomes displayed specific tumor accumulation according to luciferase expression, non-targeted liposomes only permitted a minimal level of accumulation. Furthermore, targeted liposome application in healthy mice did not generate a luciferase signal, suggesting a high tumor tissue specificity of the developed system.

Finally, Song *et al* used the integrinβ_6-targeted immunoliposomes developed by Liang *et al* (Section 2.3) to load integrinβ_6 siRNA [163]. Intratumoral administration of both targeted and untargeted immunoliposomes of around 400 nm demonstrated antitumor activity in an HT-29 human colon cancer xenograft model, although targeted liposomes produced a suppression in tumor growth ~1.4-fold higher.

3.3. Inorganic nanoparticles.

Integrin targeted-inorganic NPs have been also explored for application in gene therapy. For instance, Zhang and coworkers developed RGD-modified GNRs loaded with DOX and PLK1 siRNA coated with a thermo-switchable p(N-isopropylacrylamide)-PEG (pNIPAAm-PEG) corona [164]. PLK1 siRNA, which silences the cell division promoter Polo-like kinase 1 (PLK1), was incorporated through smart DNA sequences known as Y-motifs that disassemble after being triggered by endogenous microRNA. After administration in mice bearing HeLa cervical tumors and multiple NIR irradiation, RGD-GNRs displayed a 4.5-fold greater accumulation in tumors when followed by irradiation. This resulted in a tumor reduction of ~84 % compared to saline group, while DOX alone reduced tumor size by only ~38 %.

In another study, Yi and coworkers functionalized GNPs with cRGDfK(CX-)-PEG-PLL bearing conjugated E6 siRNA [165]. The E6 protein is important in cervical cancer as it inactivates the p53 tumor suppressor protein. The study assessed functionalized GNPs of 40 nm in mice bearing HeLa tumors, where they found greater tumor accumulation (~2.5 more at 2h) for targeted compared to non-targeted GNPs. Moreover, targeted GNPs permitted more efficient gene silencing and tumor inhibition (~2.8, and 1.7-fold less tumor volume compare to saline and untargeted, respectively) with no signs of toxicity.

Summarizing Section 3 and considering the described integrin-assisted gene therapy examples (Table 2), the vast majority of cases discussed utilized a cyclic version of RGD, as also seen in Section 2. Around one third of the examples did not make a direct comparison with untargeted analogues (only with free siRNAs or targeted constructs with control siRNAs), making conclusions on the effects of targeting a difficult task. Nevertheless, in almost all cases where this comparison was performed, it was demonstrated an enhanced *in vivo* results as a consequence of RGD introduction. Hence, the use of integrin-targeting agents correlates to the increased therapeutic potential of gene-delivery systems.

4. Integrin-assisted nanomedicines for Imaging and theranostics.

Other than treatment strategies, nanomedicines have been also proposed as nanoprobes for molecular diagnostics or to monitor disease progression by means of tracer probe labeling [166-174]. An even more interesting concept is the application of "theranostics" (therapeutic + diagnostic), which offer the possibility of early detection, disease targeting, treatment, and disease progression monitoring following treatment [175-177]. Indeed, the use of targeted nanomedicines in theranostics has recently been extensively reviewed [178-180].

Given their overexpression in cancer cells, their role in angiogenesis, and their accessibility to extracellular ligands, integrins have also been extensively investigated for uses in imaging and theranostics. Indeed, the clinical development of integrin-assisted nanoprobes are at a more advanced stage (two ongoing clinical trials of RGD-targeted nanoprobes [45, 46]) than nanomedicines aimed solely at therapeutic applications, perhaps due to less strict regulatory demands. Furthermore, commercially available RGD-bearing nanoprobes can also be found for *in vivo* experimentation purposes. Nonetheless, whether integrin-assisted nanoprobes will successfully enter the market remains to be seen, as an example of this strategy has yet to be approved by the Food and Drug Administration (FDA) for clinical use [181, 182].

4.1. Polymer-based nanoconstructs

In order to improve the generally poor pharmacokinetics of cRGDyK radiotracers (mainly due to short half-life, rapid tumor tissue clearance, apart from high kidney and liver uptake), Chen *et al* introduced a PEG spacer to create ^{18}F-Fluorobenzoil-PEG-RGD [183] and ^{125}I-PEG-RGD tracers [184]. Micro-PET (in the case of ^{18}F), autoradiography, and direct tissue sampling were used to study tumor targeting and pharmacokinetics of PEGylated-RGD *vs* non-PEGylated sequences in a U87MG glioblastoma subcutaneous mouse xenograft model, and in the case of ^{18}F experiments, an orthotopic model. From those studies, the authors concluded that PEGylated sequences exhibited greater and faster tumor

accumulation (5.2±0.5%ID/g at 30 min post-injection in case of ^{18}F probe and very similar in ^{125}I), moderate tumor clearance, and high tumor-to-background ratio when compared to the free sequences.

In another study, Chen and coworkers [185] conjugated cRGDy(ε-acetylthiol)K (9 molecules/carrier) and a fluorescent Near Infrared (NIR) dye (IRDye800) to HSA and performed an exhaustive comparative study between cRGD-HSA, cRAD-HSA (as negative control), and free cRGD probes. Their NIR fluorescence imaging (both *in vivo* and *ex vivo*) studies, confirmed by histology, revealed (i) an increase in half-life (from 2 to 20 min for free and conjugate RGD, respectively), (ii) higher specificity of the cRGD-HSA conjugate with higher tumor accumulation (6.1-fold increase compared to free cRGD probe at 24 h), and (iii) better tumor-to-background contrast when compared to RAD based conjugates and free cRGD probes. Likewise, Ma and coworkers conjugated an RGD-A7R [186] motif to radiolabeled ^{18}F-n-BSA [187]. Nanosystems of 20 nm size and an RGD content of 10-20% w/w were evaluated *in vivo* in terms of biodistribution and pharmacokinetics. The ^{18}F-n-BSA–RGD-A7R conjugate displayed greater tumor accumulation (up to 2.72 %ID/g tissue at 30 min post-injection) than free ^{18}F-RGD-A7R (~1.85 %ID/ g tissue at 30 min) and better tumor-to-background ratios.

Alternatively, Ke *et al* applied T1 mapping, a quantitative magnetic resonance imaging (MRI) technique, which allows measurement of the T1 values of water protons of different tissues, to detect $\alpha_v\beta_3$ integrin. For this purpose, they employed cRGDfK-PGA-Gd(III)-DO3A [188] bearing ~40 % w/w RGD conjugated through a long spacer to facilitate receptor interaction. This polymeric conjugate demonstrated better *in vivo* performance as compared to the free RGD peptide in a DU145 xenograft model due to the possibility of using lower Gd-equivalents giving greater tumor specificity, thus, reducing background signal. Two years later, Zarabi *et al* [189], used the same T1-mapping technique and strategy for pHPMA. The authors conjugated 0.425 mmol/g polymer of cRGDfK and introduced the Gd contrast agent as a DOTA chelate in this case. The *in vivo* studies performed in a MDA-MB-231 breast cancer xenograft model demonstrated significant tumor accumulation of the targeted DOTA-Gd conjugate (lower T1 values 2h after administration). The same authors had previously tested a pHPMA-cRGDfk-CHX-A"-DTPA-^{111}In [190] with relatively high loading of DTPA chelating agent finding kidney accumulation and a loss of tumor targeting in the same animal model. These results indicate the influence of the nature and loading of other components on the nanostructure in the final *in vivo* fate.

Mitra *et al* used their ^{99m}Tc-labeled and targeted pHPMA-^{99m}Tc-RGD4C copolymer (~16 molecules per chain) system to introduce ^{90}Y by chelation with modified DTPA residue [191, 192]. Biodistribution studies and antitumor activity performed in a DU145 human prostate carcinoma xenograft model demonstrated elevated tumor accumulation (4.32 +/-0.32 %ID/g tissue) at 72 hours after i.v. injection. More importantly, they observed a 63% decrease in tumor volume while control tumors grew up to

442% compared to baseline. The potential of pHPMA-RGD copolymers as imaging agents was also demonstrated using PET radiotracers. Yuan and coworkers developed pHPMA-cRGDyK-DOTA-^{64}Cu copolymers (7.8 %mol RGD) and used a microPET scanner to visualize and compare the tumor accumulation of targeted and non-targeted polymers in a PC3 human prostate cancer xenograft model [193]. Three hours after i.v. administration, they observed a 2.14 fold increase in tumor accumulation for the integrin-targeted construct compared to the untargeted system.

Boswell *et al* [194] synthesized cRGDfK-PAMAM dendrimers with 1.5-2.6 peptide units, labeled with Alexa Fluor 594 and DTPA-Gd(III) or ^{111}In for multimodal imaging. *In vivo* biodistribution in M21 melanoma tumor-bearing mice revealed greater tumor accumulation of the RGD bearing system. Nevertheless, unspecific accumulation in other healthy organs also occurred. Similarly, a cRGDfK–PEG–G5-PAMAM–Cy5.5 macromolecular probe has recently been developed and evaluated by Li *et al* [195] for the imaging of 4-nitroquinoline 1-oxide (4-NQO)-induced neoplasms with the aim of early detection of esophageal squamous cell carcinoma (ESC). This probe contained a molar ratio of RGD-PEG-PAMAM of 7:15:1. *Ex vivo* NIR fluorescence studies confirmed by histological analysis demonstrated that the targeted nanoprobes detected both large and small neoplasms with enhanced target-to-background ratio when compared to the untargeted probe.

Sun and coworkers prepared cRGDyK functionalized biodegradable hyperbranched polymer (c-RGD-HB-POEGMA-Gd(III)-DTPA) of 42 nm size and slightly negative z-potential [196]. Targeted and untargeted nanoprobes showed 3-fold more T1 relaxivity compared to unconjugated DTPA-Gd and greater tumor accumulation when tested in U87 tumor-bearing mice. While the targeted nanoprobes appeared to provide better results, differences were not statistically significant.

In another study, Kawamura *et al* developed integrin-targeted hollow nanocapsules formed by cross-linked polyion complex vesicles (PICsomes) [197]. Briefly, systems comprised block aniomers of PEG-b-poly(aspartic acid) derivatives and polyaspartamide-based catiomers. cRGDfK units introduced in the deprotected acetal binding sites (20, 40, and 100% mol substitution) led to the generation of ~100 nm PICsomes. Intravital microscopy indicated accumulation in the tumor neovasculature (up to 3% ID/g tumor) and, following loading with superparamagnetic iron oxide nanoparticles (SPIOs) for MRI imaging, efficient accumulation in the tumor neovasculature of orthotopic glioblastomas.

Guan *et al* developed imaging-guided chemotherapy using dextran-based micelles [198]. The authors co-assembled 20% cRGDfK-dextran and 80% Bodipy-NIR-dextran polymers in the presence of CDDP to crosslink the hybrid micellar system and generate particle sizes of ~170 nm in diameter. The study observed enhanced tumor accumulation and lower tumor-to-background noise in an EMT6 mouse

mammary carcinoma model. However, RGD-targeted micelles only provided a non-significant improvement in antitumor activity when compared to the untargeted system.

4.2. Liposomal formulations

The first integrin-targeted MRI contrast agent was a Gd(III)-labeled liposome developed by Sipkins *et al* in 1998 [199]. This system was functionalized with the monoclonal antibody LM609 that targets $\alpha_v\beta_3$ receptor and this permitted an enhanced MRI signal when applied in rabbit carcinoma tumors. More elegant strategies for angiogenesis imaging using liposomal formulations followed soon after. For instance, a multitarget and synergistic approach by Kluza *et al* [200] led to the development of Gd(III)-DTPA bearing liposomal contrast agents carrying two targeting and therapeutic peptides: 3 μg/mol lipid of cRGDf(-S-acetylthioacetyl)K for $\alpha_v\beta_3$ receptor and 10 μg/mol lipid of Anginex which targets Galectin-1. Galectin-1 is involved in endothelial cell proliferation, migration, and apoptosis [201, 202]. Liposomes composed of PC/Chol/DSPE-PEG units of 150 nm size were tested in B16F10 melanoma bearing mice [203] where, unfortunately, the results suggested short half-lives and no special benefits from this dual targeting approach, while comparisons with untargeted liposomes were not performed.

Rangger *et al* studied the influence of RGD loading in 100 nm liposome targeting by using (^{111}In)-radiolabeling with different PEG blocks and cRGDyV concentrations (from 0.06 to 6% mol) [204]. Although *in vitro* data suggested that integrin-targeting was improved by increasing RGD loading and worsened by PEGylation, *in vivo* results in different xenografts indicated only a limited level of tumor accumulation. These results exemplify the poor correlation between *in vitro* data in single cell lines with the complex *in vivo* scenario.

In another study, Sonali *et al* recently reported an RGD-TPGS bearing liposome containing both DTX and quantum dots (QDs of CdSe/ZnS) for brain cancer theranostic applications [205]. Theranostic liposomes of 182 nm contained 0.3% w/w of RGD peptide and *in vivo* biodistribution performed in healthy rats displayed a 6.5-fold higher brain accumulation for targeted compared to untargeted liposomes and Docel™ after 2 h of treatment. Further experiments assessing *in vivo* antitumor efficacy will hopefully realize the full potential of these systems.

4.3. Inorganic Nanoparticles

A vast amount of integrin-targeted INPs have been reported as imaging agents [206, 207] and so, only the most recent and relevant examples of Cornell dots (“C-dots”), magnetic INPs, MSNPs, and Au-NPs will be discussed in this section.

The Kiessling lab developed the first integrin-targeted INP, an RGD-conjugated ultra-small superparamagnetic iron oxide nanoparticle (RGD-USPION), in 2007 [208]. This probe was cell internalized and accumulated in U87MG tumors *in vivo*, although the group also observed high non-specific accumulation. Since this time, the field has rapidly and widely expanded regarding imaging [209, 210] and diagnostics [211]. Indeed, there are two ongoing clinical trials of integrin-targeted INPs, involving both the use of fluorescence core-shell silica NPs and C-dots [212]. The first system in clinical trials comprises ^{124}I-cRGDY–PEG–C dots (6-7 nm) with 6-7 ligands/particle and an encapsulated Cy5 dye [47]. In an initial *in vivo* study, Bradbury *et al* administered this construct to a spontaneous melanoma miniswine model for sentinel lymph node (SLN) mapping [47]. C-dots distinguished between inflamed and metastatic areas whereas the ^{18}F-fluorodeoxyglucose (^{18}F-FDG, current standard method used in the clinics) did not. The first-in-human study established a body half-life of the same compound administered to patients with various cancers of between 13 and 21 h [46] with mainly renal excretion and acceptable toxicity for trial advancement. A second trial aiming to use this probe to investigate radiation dosimetry, tracer tissue distributions, and PET/CT imaging of patients with malignant brain tumors is currently at the planning stage [45].

Recently, Kazmierczak successfully used a commercially available RGD-USPION for MRI visualization of angiogenesis during treatment with bevacizumab in an orthotopic MDA-MB-231 breast cancer xenograft model [213]. The nanosized probe of ~360 nm diameter containing RGD (3500 unit/INP) tracked angiogenesis inhibition upon treatment despite its very short half-life (about 6 min). Similarly, the RGD-PEG-USPION developed by Luo *et al* for T_1-weighted MR imaging of gliomas demonstrated significantly higher tumor accumulation in U87MG glioma bearing mice compared to untargeted SPIONS [214]. In another study, Zhang and coworkers developed dual-targeted PEG coated 8 nm SPION modified with both cRGDyK and folic acid (FA) at high and low target loadings [215]. When administered in C6 glioma bearing mice, they observed an increased signal-to-noise ratio for the dual-targeted SPIONs by MRI (54% and 31% for high and low loadings, respectively) as compared to single-targeted (~18%) and non-targeted SPIONS (~9%). In this case, dual targeting and increased RGD loading improved tracer potential.

Alternatively, Richard and coworkers investigated cRGDfK-PEG-PO/γFe_2O_3 INPs (~80 nm diameter) for MRI imaging in U87-MG human glioma xenograft [216]. Systems containing 17±9 RGD/INP demonstrated high transverse relaxivity for both targeted and untargeted systems and while tumor-specific accumulation was observed at 1 day post-injection, the study did not provide an *in vivo* comparison to an untargeted control. Kitagawa and coworkers developed human ferritin (HFn) and RGD4C conjugated Fe_3O_4 NPs of 12 nm to improve MRI imaging of angiogenesis and inflammation in murine models of carotid disease and abdominal aortic aneurysms (AAA) [217]. In both cases, targeted

INPs performed better than untargeted INPs with 1.9 and 2.3-fold higher signal intensity loss in carotid and AAA diseases, respectively. Wang *et al* used 40 nm ^{125}I-cRGDyK-PEG-MNPs (magnetic nanoparticles) of Fe_3O_4 for MR and SPECT imaging to direct photothermal therapy [218]. Both biodistribution studies demonstrated selectivity of the targeted probe, whose maximum signal was detected at 6 hours (6.75 %ID/g) in SPECT, and effective blocking by pre-injection of RGD. The system was used for MR/SPECT guided PTT and detected disease progression upon tumor irradiation up to 16 days, at which point tumors were completely destroyed. Additionally, the use of targeted cRGDyK-PEG-MNPs with laser treatment increased tumor cell apoptosis (47.7%) when compared to cRGDyK-PEG-MNPs alone (24.1%) and saline plus laser irradiation (29.9%). However, the study failed to perform a comparison with the untargeted system.

In another study, Huang and coworkers utilized surface-enhanced resonance Raman spectroscopy (SERRS) to visualize the spread of glioblastoma in a transgenic model of murine glioma [219]. Au-NPs of 60 nm were coated with silica and modified with cRGDyK-PEG or cRADyK-PEG and different dyes (IR792 or IR780). SERRS was performed in fixed brains after co-injection of both RGD/RAD bearing sequences demonstrating that integrin-targeted NPs detected the margins of the tumor area when compared to RAD-bearing NPs and distal tumor cells not detected by RAD-SERRS. Nevertheless, this technique does not permit non-invasive *in vivo* imaging.

Yang and coworkers compared cRGDyC-Au-NPs-Gd^{99m}Tc to RADyC-Au-NPs-Gd^{99m}Tc with different RGD loadings (from 350 to 1500 unit/NP) and different diameters (29, 51, 80 nm) as probes for MRI and/or SPECT/CT [220]. T1-weighted MRI images showed higher tumor accumulation for targeted NPs of 29 nm when injected in mice bearing H1299 tumor cells. SPECT/CT and post-mortem quantification confirmed the MRI results, where targeted NPs exhibited 14 %ID/g in tumors whereas RAD-NPs exhibited only 4% ID/g. Moreover, the therapeutic efficacy of Au-NPs in radiotherapy tested using 10 GY of γ-rays demonstrated higher dsDNA damage for targeted compared to untargeted NPs. Zhang and coworkers prepared GNRs coated with polydopamine (PDA) and PEG, further functionalized with cRGDyC (58 unit/INP) and ^{125}I, and loaded with CDDP as a theranostic agent for chemo/photothermal therapy (PTT) and SPECT/photoacoustic imaging (PAI) [221]. Mice bearing H1299 lung cancer tumors were treated with these systems and RAD-analogues. Targeted GNRs accumulated 3.23-fold more in tumor tissue than untargeted GNRs as determined by SPECT and confirmed by PAI. The combination of chemo/photodynamic therapy was then applied, demonstrating that targeted GNRs (loaded or not with CDDP) completely destroyed tumors while free CDDP-treated tumors increased in size by ~34%.

Zeng and coworkers used NIR fluorescence molecular imaging (FMI) for intraoperative imaging of liver cancer microfoci using RGD-MSNPs loaded with Indocyanine green ICG dye [222]. This method aided in

the delineation of liver cancer margins in mice bearing MDA-MB-231-fLuc metastatic breast tumors as well as the identification of satellite lesions of <1 mm. In this study, RGD-MSNs outperformed non-targeted MSNs both *in vitro* and *in vivo*. Alternatively, Chen and coworkers developed core-shell Fe_3O_4 magnetic MSNPs (MMSNPs) functionalized with GRGDS-β-cyclodextran (CD) connected via a platinum IV prodrug (2.4% w/w) and loaded with DOX (5.4% w/w) resulting in ~160 nm multifunctional INPs [223]. Targeted MMSNPs accumulated at the tumor site significantly better (~1.5-times) than untargeted according to MRI after i.v. injection in mice bearing HeLa tumors. Furthermore, application of a magnetic field additionally increased uptake and improved tumor-to-background in MRI images by decreasing non-specific accumulation (Figure 4). Finally, apoptosis levels in tumors treated with RGD-MMSNs were significantly higher (41.2%) than non-targeted (15.7%) or free DOX (18.9%) and were further increased upon addition of a magnetic field (up to 68%).

Finally, Gao and coworkers were able to treat deep-seeded tumors by photodynamic therapy (PDT) through the use of near-IR up-conversion NPs (UCNPs) which convert near-IR light to visible light, thereby activating an encapsulated photosensitizer. ICG and ZnPc loaded cRGDyK-CS-$NaYF_4$:Yb,Er NPs of 52 nm were prepared and tested in mice bearing PC-3 prostate tumors [224]. RGD-UCNPs accumulated in the tumors at earlier time points than UCNPs (4 *vs* 8 hours post-injection) as visualized by *in vivo* FOI. PDT using these targeted systems sensitized tumors prior to the administration of Doxil® and this two-step treatment resulted in a tumor inhibition rate of 79% compared with 56% after Doxil treatment alone. The study attributed these results to enhanced tumor accumulation of the chemotherapeutics when administered after PDT.

From the examples provided in Section 4, including all integrin-assisted nanomedicines for imaging and theranostics regardless of the nature of the carrier (see Table 3), we can draw similar conclusions as for Sections 2 and 3. The use of cyclic RGD sequences predominates over linear sequences and, as a general trend, RGD-nanoprobes exhibited improved *in vivo* performance when compared to free RGD-probes or untargeted constructs. Although there are fewer examples of theranostic agents, almost all of those assessed resulted in enhanced antitumor activity upon integrin targeting. Thus, the illustrations provided in this section highlight the potential use of these targeted systems as imaging nanoprobes and as theranostic agents. Indeed, we note that this area of application is the most advanced of its kind in clinical development.

5. Conclusions and future directions.

As indicated by the wide variety of examples reviewed here, the use of integrin-targeting ligands and antibodies has been widely explored at the research level since the 1990's and many of these

nanosystems demonstrate enhanced biological performance in the field of cancer imaging and/or treatment. Moreover, due to integrins role in cancer progression and metastasis, the use of these moieties can provide beneficial effects, acting as anti-metastatic activity. Despite a wealth of promising preclinical data, only two clinical trials using integrin-targeted sequences are ongoing [45, 46] and limited examples of targeted systems in general have reached this status [182]. Indeed, there still exists room for improvement in the design of integrin-targeted nanomedicines at the preclinical level. Special attention should be given to the techniques used to assess nanomedicine-specific targeting. These studies require reliable *in vivo* models, which highly resemble human scenarios, the performance of adequate *in vivo* quantification, and the application of experimental conditions involving blocking assays to confirm tumor targeting. Furthermore, *in vitro* targeting is often not directly translated to *in vivo* specificity as many integrins are ubiquitous receptors of endothelial cells, and therefore sufficient tumor-to-other tissue receptor expression ratio measurements are required.

Important to note, the design of ligands with enhanced integrin avidity and stability is still under investigation, where the use of more hydrophobic sequences and appropriate spacers can significantly increase the targeting properties [26, 225]. This research should be always combined with the study of the biological processes underlying integrin targeting, receptor blocking, and recycling depending on the pathological conditions to properly apply a reiterative design. As mentioned in the introduction, many factors must be taken into consideration when designing a ligand-targeted nanomedicine including carrier type (size, shape, charge, deformability…), ligand density as well as tumor type (vascularity and permeability), and tumor stage. Not only that, as very recently demonstrated, the differential expression of integrins in tumor-derived extracellular vesicles is a cell-intrinsic determinant of organ tropism in metastatic processes[15, 227]; so the RGD-bearing peptide sequence and its arrangement in the nanocarrier is of critical importance. It is envisage that integrin targeting will not only have an impact on targeting metastatic processes but also, if such tropism is well understood, integrin-assisted targeting could even be used to block key metastasis progression due to its direct modulation with the metastatic niche conditioning.

Specific integrin expression in liquid biopsies could be even used as biomarker to predict tumor metastasis and recurrence in certain tumors yielding towards personalized medicine strategies, including companion diagnosis. Examples of new molecular PET and MRI tracers bearing peptides targeting integrins are in an advanced stage of development as these probes do not only address surface proteins but also cell interaction, migration and invasiveness events [226,228] and if well-understood, they could be applied as the basis of personalized approaches allowing patient stratification as well as more defined therapeutic strategies.

From the lessons learned in the field of nanomedicine, it is clear that many critical issues should be addressed before moving to clinical translation. Previous failures have evidenced that one of the biggest gaps between the laboratory and the clinic is the need for reproducibility and the feasibility of large-scale production. For this reason, the mantra "the simpler, the better" should be headed. Less complex systems will receive more interest from the pharmaceutical industry due to fewer costs and complications in upscaling. The incorporation of targeting ligands (especially antibodies) introduces additional complexity and costs to a nanoconstruct, and therefore, their final benefits should be overtly demonstrated in order to be worthy of industrial development. In spite of needing further developmental improvements, targeted nanomedicines including those integrin-assisted are still envisaged as star candidates for highly specific and personalized medicine with reduced toxicity and side effects.

FIGURE CAPTIONS

Figure 1. Schematic representation of the most commonly employed RGD peptidic sequences

Figure 2. A) Schematic representation of the self-assembly of the polymeric prodrug platform [a) Drug, b) Stimuli-responsive bond, c) Chain-breakage functionality, d) Hydrophilic moiety, e) RGD-ligand] **B**) Tumor volume of HepG2 tumor-bearing mice after i.v. administration of free HCPT (black), RGD-NPs (red), RGD-NPs lacking fast responsive linker (blue), and PBS control (pink). n.s. non-significant. **C**) Images from HepG2 tumor-bearing mice after treatments. Reproduced with permission from Xu *et al*, see reference for more information.

Figure 3. Structures of PEGylated RGDK-Lipopeptide 1 and PEGylated RGEK-lipopeptide 2 (**A**). Intravenous administration of CDC20 siRNA encapsulated within the liposomes of PEGylated RGDK-lipopeptide 1 significantly inhibits melanoma tumor growth (**B** and **C**) in a syngeneic mouse tumor model after multiple treatments (days 12, 14, 16, 18 and 20 post-tumor inoculation) and downregulates expression of CDC20 in tumor tissues (**D**). Reproduced with permission from Majumder *et al*, see reference for more information.

Figure 4. **A**) Schematic representation of the design and proposed mechanism for MMSNPs as theranostic agents. **B**) *In vivo* non-invasive MRI imaging of HeLa tumor-bearing mice before and after treatment with Integrin-targeted Pt(IV)-containing MMSNPs (a, and b) and non-targeted MMSNPs (c, and d). Two tumors were inoculated (white arrows) and magnetic targeting with an external magnet performed on the right tumors only. a and c are T2-weighted MRI images and b and d, their respective

pseudo-color representations. **C**) HeLa tumors obtained and **D**) TUNEL-positive cell percentages after i.v. treatments with PBS, DOX, Pt(IV) containing-MMSNPs with and without RGD-ligands and Pt(IV) containing-RGD-MMSNPs with an external magnet (M). Reproduced with permission from Chen *et al*, see reference for more information.

Acknowledgements

The authors acknowledge Stuart P. Atkinson for English editing and Inmaculada Conejos-Sánchez for her help in the figures. The Spanish Ministry of Economy and competitiveness (Grants SAF2013-44848-R and SAF2016-80427-R) and the European Research Council (Grants ERC-CoG-2014-648831 [MyNano]) are acknowledged for financial support.

Table 1. Integrin-assisted drug delivery systems.

Type	Composition	Peptide sequence (loading)[#]	Drug (loading)[#]	Size[ł]/z-pot	*In vitro**	*In vivo**	Mice Model	Ref
P-C	PEG	YIGSRG, GRGDS (100-300 μmol/g)	RGD itself	n.d./n.d.	+	+	B16-BL6 melanoma	[56-58]
P-C	PEG	(RGDT)n	RGD itself	n.d./n.d.	+	+	B16-BL6 melanoma	[59]
P-C	p(CEMA)	RXDS, x=G, L, I (50% w/w)	RGD itself	n.d./n.d.	n.d.	+	B16-BL6 melanoma/L5178Y-ML25 lymphoma	[60, 61]
P-C	Chitin	RGDS (25% w/w)	RGD itself	n.d./n.d.	n.d.	+	B16-BL6 melanoma/L5178Y-ML25 lymphoma	[62, 63]
P-C	PEG	$c(RGDfK)_2$ (1 unit/pol)	hyd-DOX (1 unit/pol)	n.d./n.d.	+	+	DA3 breast cancer	[64]
P-C	PGA	$c(RGDfK)_2$ (24-28% w/w)	PTX (24-28% w/w)	7nm/n.d.	+	+	4T1 breast cancer	[65]
P-C	pHPMA	RGDfk (~5 % w/w)	DTX (~% 7w/w)	3nm/n.d.	=	=	DU145 prostate cancer	[67]
P-C	pHPMA	RGDfK (6.1 unit/pol)	AH-GDM (10.8 % w/w)	n.d./n.d.	+	+	DU145 prostate cancer	[68-70]
P-C	PEG-PAMAM	cRGDyC (16.8 unit/pol)	DOX (14.2 units/pol)	17nm/n.d.	+	+	B16 melanoma, C6 glioma	[74, 75]
P-C	PEG-PAMAM	iRGD (10.1 unit/pol))	DOX (11.9 units/pol)	20nm/2.45mV	+	+	C6 glioma	[76]
P-C	PEG-PAMAM/PLGA-PLA	cRGDyC (10 unit/pol)	DOX (13 units/pol)	n.d./n.d.	+	+	C6 glioma	[77]
P-C	PEG-PAMAM/MSCs	cRGDyC (16.8 unit/pol)	DOX (14.2 units/pol)	n.d./n.d.	=	=	C6 glioma	[78]

Pol. Drug	HCPT pol	GGRGD (10%mol)	10-HCPT (36 % w/w)	70nm/n.d.	+	+	HepG2 tumor	[79]
Psome	PEG-b-PCL	cGRGDSPK (6.5% mol)	OM (6.8 %)	95nm/n.d.	+	+	Bile duct ligation induced liver fibrosis in rat	[81]
Psome	POEGMA-PDPA	iRGD ($1.6{\cdot}10^3$ unit/psome)	PTX (~10^5 unit/psome)	214nm/0mV	+	+	Gastric (MKN-45P)/colon (CT26) peritoneal tumors	[82]
Psome	Pluronic F127	cRGDyK (n.i.)	PTX (1.54 %), DOX (1.03%)	23nm/0mV	+	+	U87MG brain glioma/MDR HSC (KBv)	[83-85]
Micelle	PLA-PEO	RGD4C (1 unit/pol)	PTX (50% w/w)	128nm^{TEM}/n.d.	+	+	MDA-MB-435 breast cancer	[86]
Micelle	PEOz-PLA	cRGDyK (0.5 unit/pol)	PTX (10% w/w)	28nm/n.d.	+	+	PC-3 prostate cancer	[87]
Micelle	PEG-PLA	cRGDyK (n.i.)	PTX (17.3 % w/w)	35nm/n.d.	+	+	U87MG glioblastoma	[88]
Micelle	PEG-PLA	cRGDyK (n.i.)	DTX (45 % w/w)	100nm/-20mV	+	+	U87MG glioblastoma	[89]
Micelle	PEG-PLA	RGD (0.24% w/w)	Curcumin (4.7%)	20nm^{TEM}/0mV	+	=	B16 melanoma	[90]
Micelle	PEO-PCCL	RGD4C (10% mol/pol)	DOX (33% of COOH)	60-90nm/n.d.	+	+	MDA-435 LCC6 derived tumors	[91]
Micelle	PEG-PGA	cRGDfK (20% mol)	(DACHPt) 0.5 %mol	30nm/n.d.	+	+	U87MG glioblastoma, melanoma LN metastasis	[92, 93]
Micelle	PEG-PGA	iRGD co-administered	CDDP (23.3 %w/w)	5-26nm/-8mV	n.d.	=	A549 NSCLC	[94]
Micelle	PEG-PLA + PEG-PAGE	cRGDfK (46% of pol units)	EPI (30% w/w)	18-60nm/n.d.	+	=	B16F10 melanoma	[95-97]
Micelle	P(OEGMA-co-BSMA)	cRGDyK (2.8%mol)	BUF (32.9% w/w)	33nm/n.d.	+	+	LoVo Colon cancer	[98]
NP	HSA	cRGDf(ε-S-ac-thioac)K (5-7 unit/pol)	MMAE/F (4.1 units/pol)	n.d./n.d.	+	+	C26 carcinoma	[99, 100]

NP	BSA crosslinked	c(RGDyK)C (n.i.)	GEM (12.8 %)	130nm/-30mV	+	+	BxPC-3 pancreatic cancer	[101]
NP	PLGA-PEG	cRGDfK (1% w/w)	Pt(IV) (1%)	120nm/-25.9mV	+	+	MCF7MFP1 breast cancer	[103]
NP	PCL-PVP	iRGD (10% surface)	PTX (15 %)	40-60nm/-5-10mV	+	+	H22 hepatic tumors	[104]
NP	Inulin	cRGDfK (n.i.)	EPI (8.1%)	150nm/n.d.	+	+	H22 hepatic tumors	[105]
NP	PEG-PTMBPEC	cRGDyK (up to 20% mol)	DOX (~10%)	181nm/-16 mV	+	+	B16 melanoma	[106]
NP	TPGS-SS-PLA	cRGDfC (1 mol %)	PTX (3.11%)	130nm/-30mV	+	+	S180- and B16F10 melanoma	[107]
Lipo	DSPE-PEG	cRGDf(ε-S-ac-thioac)K (~300 unit/lipo)	DOX (80–150 μg/μmol lipid)	n.d./n.d.	+	+	C26 carcinoma	[109]
Lipo	PC/DSPE-PEG	RGDm (~1800 unit/lipo)	DOX (1:15 wt/wt lipid)	120nm/n.d.	+	+	B16 melanoma	[110]
Lipo	PC/DSPE-PEG	RGD (24.5%mol/mol DSPE-PEG)	DOX (1:15 wt/wt lipid)	120nm/-1.4 mV	+	+	B16 melanoma	[111]
Lipo	PC/Chol/DSPE-PEG	RGD (5% mol/mol lipid)	PTX (n.i.)	117 nm/n.d.	+	+	SKOV-3 ovarian cancer	[112]
Lipo	PC/Chol/DPPE-PEG	Ac-PHSCNK-NH_2, (n.i.)	DOX (5.2% wt)	96nm/-3.5mV	+	+	B16F10 melanoma	[113, 114]
Lipo	PC/Chol/DSPE-PEG	cCDGF(3,5-DiF)G-Hyp-NC, (45%mol/mol DSPE-PEG))	DOX (1:15 wt/wt lipid)	100nm/-2.5mV	+	+	MDA-MB-231 breast cancer	[118]
Lipo	PC/Chol/DSPE-PEG	cRGDyk (8.6%mol/mol DSPE-PEG)	PTX (n.i.)	95nm/-2.63mV	+	+	PC-3 prostate cancer	[119]
Lipo	PC/Chol/DSPE-PEG	cRGDfC (1:6 mol/mol lipid)	EPO906 (0.1-100 nM)	100nm/n.d.	+	=	Kelly neuroblastoma, RH-30 rhabdomyosarcoma	[120]

Lipo	PC/Chol/DSPE-PEG	TR (cRGDfKC + TH) (n.i.)	PTX (3.2%)	110nm/-14 mV	+	+	C6 glioma	[121]
Lipo	Lecithin/Chol/DSPE-PEG	Ac-CRGDS (5% w/w)	CD-PFD (8.8 %), GEM (14.6 %)	70nm/-30mV	+	+	PSCs/Panc-1 pancreatic cancer	[122]
Lipo	Fatty alcohols	RGDF (5% mol)	DOX (5.3 %)	150-230nm^{TEM}/-50mV	n.d.	+	S180 sarcoma	[123]
Lipo	Fatty alcohol	RGDX X:-,F,V (5% mol)	DTX (1:0.5 DTX:RGD w/w)	240nm^{TEM}/-50mV	+	+	S180 sarcoma	[124]
Lipo	DSPE/Chol/CHEMS	RGD (1:1 CHEM/CHEM-RGD)	DTX (8%)	130nm/-26mV	+	+	MCF-7 breast cancer	[125]
Lipo	PC/Chol/DSPE-PEG	cRGDfKC (6% mol)	DTX (4.3%)	146nm/-30mV	+	+	MCF-7 breast cancer	[126]
Lipo	PC/Chol/DSPE-PEG	mAb E7P6 (n.i.)	5-FU (n.i.)	405nm/-8mV	+	+	HT-29, SW480β6 colon cancer	[127]
Hyb Mic	TPGS + DSPE-PEG	cRGDfC (5:1 w/w TPGS:DSPE-PEG-RGD)	DOX (n.i.)	150nm/n.d.	n.d.	=	MCF-7/breast/B16F10 melanoma/H22 hep. carcinoma	[128]
Hyb Mic	C_{16} or C_{18} F.A.	RGD or cRGDfK (1 unit/F.A.)	PTX (0.7-1 mol)	140-300nm^{TEM}/n.d.	+	+	A2058 Melanoma	[129, 130]
Hybrid NP	DSPE-PEG/lecithin/PLGA	RGD (n.i.)	DTX (n.i.)	110nm/-25mV	+	+	C6 GBM (rat)	[131]
Hybrid NP	DSPE-PEG/lecithin/PLGA	Folic acid cRGDfK (n.i.)	PTX (n.i.)	n.d./n.d.	+	+	T98G glioblastoma	[132]
INP	PAA/CS MSNPs	cRGD (n.i.)	TPT (1.8 %), QT (1.2%)	65–75nm/42mV	+	+	MDA-MB-231 breast cancer	[136]
INP	MSPNs	$(RGDWWW)_2KC$ (n.i.)	DOX (4.36 %)	128nm/n.i.	+	=	H22 hepatic tumor	[137]
INP	MSNPs	cRGDfC (n.i.)	GNRs/X-ray	80nm^{TEM}/17mV	+	+	MDA-MB-231 breast cancer	[138]
INP	MSNPs	cRGDfK (0.20 mmol/g)	ATO (0.61 mmol/g)	100nm^{TEM}/n.d.	=	+	MDA-MB-231 breast cancer	[139]

INP	PEG-GNR	FITC-GARGDLASLC, GGGGG (n.i.)	GNRs/X-ray	40x9.3nm^{TEM}/−12mV	+	n.d.	HSC3 oral cancer	[140]

[#]The amount of peptide sequence and drug loading was used as provided or calculated from the published data where possible. Ł Size is provided as hydrodynamic diameter obtained by Dynamic Light Scattering (DLS) unless indicated with the superscripts TEM (for Transmission Electron Microscopy). *Efficacy (accumulation, antitumor activity, or anti-metastatic activity) compared to non-targeted/random targeted or free peptide: Improved (+), comparable (=), worsened (-), not determined (n.d.) 5-FU: 5-fluorouracil, BSMA: 3-((2-(methacryloyloxy)ethyl) thio)propanoic acid, ATO: arsenic trioxide, EPO906: Patupilone, F.A.: Fatty acid, FITC: Fluorescein isothiocyanate, HSC: Human squamous carcinoma, Hyb: Hybrid, Lipo: Liposome, LN: Lymph node, mAb: Monoclonal antibody, , n.d.: Not determined , n.i.: Not indicated , NSCLC: Non-small-cell lung carcinoma, OM: Oxymatrine, P-C: Polymer Conjugate, PFD: Pirfenidone, Pol. Drug: Polymeric Drug, PSCs: Pancreatic stellate cells, Psome: Polymersome, Pt: Platinum, QT: quercetin, TPT: topotecan. The rest of the abbreviations can be found in the general abbreviation list.

Table 2. Integrin-assisted gene delivery systems

Type	Composition	Peptide sequence (loading)[#]	Nucleotide	Size/z-pot	*In vitro**	*In vivo**	Animal Model	Ref
Polyplex	$(K[H-]KKK)_6$	cCRGDCF (1 unit/oligolysine)	pCMV-Luciferase	n.d./n.d.	+	n.d.	Mice: PLC hepatoma, MIAPaCa-2 pancreatic cancer	[143]
Polyplex	G1-PAMAM	cRGDfC (2.6 %)	pVEGF165 gene	80-160nm/3-20mV	+	+	Rabbit: injured carotid artery model	[144]
Polyplex	PEI-PEG	cACRGDMFGCA (40 unit/PEI)	VEGF R2 siRNA	100nm/6mV	+	+	Mice: N2A neuroblastoma mice	[145]
Polyplex	PEI-PEG	cACDCRGDCFC (1.3 unit/PEI)	pCMV-sFlt-1	100-200nm/32mV	+	+	Mice: CT-26 colon adenocarcinoma	[146, 147]
Polyplex	PEI-PEG	cACDCRGDCFC (1.3 unit/PEI)	VEGF R1 siRNA	160nm/4-6mV	+	+	Mice: CT-26 colon adenocarcinoma	[148]
Micelle	Pluronic 123	cRGDfK (1 % w/w)	pCMV6-AP-2α	20nm/n.d.	+	+	Mice: MGC803 gastric tumor	[149]
NP	PEO-b-P(CL-g-SP)	RGD4C (32 unit/NP)	MCL-1 siRNA	60-70nm/~-2mV	+	+	Mice: MDA-MB-435 melanoma	[150]
NP	PLGA	GRGDSPK (0.62% w/w)	STAT1 mRNA	250nm/0mV	+	+	Mice: Collagen-induced arthritis (CIA)	[151]
NP	TPGS/Pluronic P85-PEI	iRGD (2%)	PTX (1.88 %), survivin shRNA	141-160nm/30mV	+	+	Mice: A549/T lung cancer	[152]
Lipid NP	Diacetylene phospholipids	Integrin synthetic antagonist (n.i.)	cDNA ATP^{μ}-Raf	n.d./n.d.	+	+	Mice: M21-L melanoma	[154]
Lipo	Chol/lip amph/lipopep	RGDK (1:0.05 chol:RGDK-lipopep)	CDC20 siRNA	160-180nm/3-4mV	+	+	Mice: B16F10 melanoma	[155, 156]
Lipo	DOTA/DOPE/DSPE-PEG	RGD (15 mol%)	PAX3-FOXO1 (P3F) siRNA/protamine	222nm/7.8nm	+	+	Mice: Rh30 alveolar rhabdomyosarcoma	[158]
Lipo	YSK05/POPE/Chol/PEG	cRGDfK (1-10% mol)	VEGFR-2 siRNA	115 nm/-18mV	+	n.d.	Mice: OS-RC-2-kidney carcinoma	[161]

Lipo	PC/Chol/DPPE-PEG	PR_b (5% mol)	pT2/Cal DNA luc/bPEI	280 nm/-3 mV	+	+	Mice: CT26 colon carcinoma	[162]
Lipo	PC/Chol/DSPE-PEG	mAb E7P6 (n.i.)	Integrin β6-siRNA	396nm/-7.65m	+	+	Mice: HT-29 colon cancer	[163]
INP	PNIPAAM-PEG-GNR	RGD (32 unit/GNR)	PLK1 siRNA, DOX (3000 unit/GNR)	n.d./n.d.	+	+	Mice: HeLa cervical cancer	[164]
INP	PEG-PLL-coated GNP	cRGDfk(CX-) (n.i.)	E6 siRNA	40nm/-11mV	+	+	Mice: HeLa cervical cancer	[165]

[#] The amount of peptide sequence was used as provided or calculated from the published data where possible. *Efficacy (accumulation, antitumor activity, or anti-metastatic activity) compared to non-targeted/random targeted or free peptide: Improved (+), comparable (=), worsened (-), not determined (n.d.). ATP-Raf: Adenosine triphosphate- Rapidly Accelerated Fibrosarcoma, CDC20: Cell-division cycle protein 20, CMV: cytomegalovirus, E6: E6-oncogene/oncoprotein, Lip amph: amphiphilic lipid, Lipo: Liposomes, Lipopep: Lipopeptide, Luc: Luciferase, MCL-1: Induced myeloid leukemia cell differentiation protein, n.d.: Not determined, n.i.: Not indicated, PAX3-FOXO1: paired box3-forkhead box protein O1, PLK1: Serine/threonine-protein kinase, POPE: 1-palmitoyl-2-oleoyl-sn-glycero-3-phosphoethanolamine, STAT1: Signal transducer and activator of transcription 1,VEGF: vascular endothelial growth factor. The rest of the abbreviations can be found in the general abbreviation list.

Table 3. Integrin-assisted nanoprobes and theranostic agents.

Type	Composition	Peptide sequence (loading)[#]	Active Agent	Dye/Technique	Size/z-pot	*In vitro**	*In vivo*[‡]	Model	Ref
P-C	PEG	cRGDyK (1 unit/pol)	--	^{18}F/MicroPET, autoradiography	n.d.	n.d.	+	U87MG glioblastoma	[183]
P-C	PEG	cRGDyK (1 unit/pol)	--	^{125}I/autoradiography	n.d.	n.d.	+	U87MG glioblastoma	[184]
P-C	HSA	cRGDy(ε-acetylthiol)K (9 unit/pol)	--	IRDye800/FOI	n.d.	+	+	U87MG glioblastoma	[185]
P-C	n-BSA	RGD-A7R (10-20%)	--	^{18}F/MicroPET/CT	20nm/0mV	n.d.	+	U87MG glioblastoma	[187]
P-C	PGA	cRGDfK (13% mol)	--	Gd(III)/T1 mapping MRI	n.d.	=	+	DU145 prostate cancer	[188]
P-C	pHPMA	cRGDfK (0.425 mmol/g pol)	--	Gd(III)/T1 mapping MRI	n.d.	=	+	MDA-MB-231 breast cancer	[189]
P-C	pHPMA	cRGDfK (0.21-0.29 mmol/g pol)	--	^{111}In/Gamma camera	n.d.	=	-	Lewis lung carcinoma (LLC1)	[190]
P-C	pHPMA	RGD4C (0.377 mmol/g pol)	^{90}Y (9.6 mCi/mg pol)	^{99m}Tc/Gamma camera	n.d.	=	+	DU145 prostate cancer	[192]
P-C	pHPMA	cRGDyK (7.8% mol)	--	DOTA-^{64}Cu/MicroPET	n.d.	n.d.	+	PC3 prostate cancer	[193]
P-C	pHPMA	RGD4C (0.5 mmol/g pol)	--	^{99m}Tc/ Gamma camera	n.d.	n.d.	+	DU145, PC-3 prostate cancer	[48, 49]
P-C	pHPMA	cRGDfK, cCNGRC (8.9% w/w)	--	DY-676/FOI	n.d.	n.d.	-	CT26 colorectal, BxPC3 prostate	[50]
P-C	PAMAM	cRGDfK (1.5-2.6 unit/pol)	--	AlexaF,Gd(III), ^{111}In/Multimodal	n.d.	+	-	M21 melanoma	[194]
P-C	PAMAM	cRGDfK (7 unit/pol)	--	Cy5.5/NIRF *ex vivo*	n.d.	n.d.	+	(4-NQO)-induced neoplasms	[195]

P-C	HB-POEGMA	cRGDyK (28.8% w/w)	--	Gd(III)/MRI	42nm/-1.26mV	=	=	U87MG glioblastoma	[196]
PICsomes	PEG-P(Asp)	cRGDfK (5-25 unit/pol)	--	SPIO/MRI	100nm/~-30mV	+	+	U87MG glioblastoma	[197]
Micelle	Dextran	cRGDfK (20%)	CDDP (15% w/w)	Bodipy-NIR/FOI	170nm/n.d.	+	=	EMT6 mammary carcinoma	[198]
Lipo	PC/Chol/DSPE-PEG	Anx, cRGDf(S-ac-thioac)K (10, 3 μg/μmol)	Anx/cRGD	Gd(III)/MRI	150 nm/n.d.	+	n.d.	B16F10 melanoma	[200, 203]
Lipo	PC/Chol/DSPE-PEG	cRGDyV (0.06- 6 mol%)	--	^{111}In/Micro SPECT/CT	100nm/-1.8-6.3mV	+	=	M21 melanoma, U87MG glioblastoma	[204]
Lipo	PC/Chol/TPGS	RGD (1.16 % of DPPC)	DTX (0.58% of DPPC)	CdSe/ZnS QDs/*Ex vivo* FOI	182nm/1.10mV	+	+	Healthy rats	[205]
INP	PEG-C-dots	cRGDY (6-7 units/INP)	--	^{124}I, Cy5.5/PET,FOI	6-7nm/n.d.	+	+	Miniswine melanoma, Human cancers	[226] [47]
INP	USPIO	RGD (3500 unit/INP)	--	SPIO/MRI	180nm/n.d.	n.d.	n.d.	MDA-MB-231 breast cancer	[213]
INP	PEG-USPIO	RGD (0.5 unit/PEG)	--	SPIO/MRI	2.7nm/-10mV	+	+	U87MG glioma	[214]
INP	PEG-SPION	cRGDyK (n.i.) and FA (n.i.)	--	SPIO/MRI	8nm^{TEM}/n.d.	n.d.	+	C6 brain glioma	[215]
INP	PEG-PO-γFe_2O_3	cRGDfK (17±9 unit/INP)	--	Iron Oxide/MRI	38.9nm/n.d.	n.d.	n.d.	U87MG glioma	[216]
INP	HFn-Fe_3O_4	RGD4C (24 unit/HFn)	--	Iron Oxide/MRI	12nm/n.d.	n.d.	+	Carotid, AAA murine	[217]
INP	PEG-Fe@Fe_3O_4	cRGDyK (n.i.)	Fe_3O_4, Irradiation	^{125}I/SPECT, Fe_3O_4/MRI	12nm/-15mV	+	+	U87MG glioblastoma	[218]
INP	PEG-Au	CRGDyK (n.i.)	--	Raman	140nm/n.d.	n.d.	+	RCAS-PDGF/N-tva murine glioma	[219]
INP	Au	cRGDyC (350, 960, 1500 unit/INP)	Au, γ-irradiation	^{99m}Tc/ SPECT/CT, Gd/MRI	29,51,80nm/n.d.	+	+	H1299 lung cancer	[220]

INP	PDA-GNRs	CRGDyC (58 unit/INP)	CDDP, Au/PTT	^{125}I/SPECT/CT/PAI	54 x 15nm/-31mV	+	+	H1299 lung cancer	[221]
INP	MSNPs	RGD (n.i.)	--	ICG/NIR-FMI	100nm/n.d.	+	+	MDA-MB-231 breast cancer	[222]
INP	MMSNPs-	GRGDS (n.i.)	Pt(IV) (2.4%), DOX (5.4%)	Fe_3O_4/MRI	163nm^{TEM}/3.3mV	+	+	Hela cervical cancer	[223]
INP	$NaYF_4$:Yb,Er CS	cRGDyK (n.i.)	ZnPc (9%), PDT	ICG/OI	52nm^{TEM}/n.d.	n.d.	+	PC3 prostate cancer	[224]

[#] The amount of peptide sequence was used as provided or calculated from the published data where possible. Ł Size is provided as hydrodynamic diameter obtained by Dynamic Light Scattering (DLS) unless indicated with the superscripts TEM (for Transmission Electron Microscopy). *Efficacy (accumulation, antitumor activity, or antimetastatic activity) compared to non-targeted/random targeted or free peptide: Improved (+), comparable (=), worsened (-), not determined (n.d.). AlexaF: Alexa fluor, Anx: Anginex, BODIPY: Boron-dipyrromethene, Cy5.5: cyanine 5.5, DPPC: dipalmitoylphosphatidylcholine, Lipo: liposomes, n.d.: Not determined, n.i.: Not indicated, NIRF: Near infrared fluorescence, OI: optical imaging, P-C: polymer-conjugate. The rest of the abbreviations can be found in the general abbreviation list.

.

References

1. Carmeliet, P., *Angiogenesis in life, disease and medicine.* Nature, 2005. **438**(7070): p. 932-6.
2. Folkman, J., *Tumor Angiogenesis: Therapeutic Implications.* New England Journal of Medicine, 1971. **285**(21): p. 1182-1186.
3. Folkman, J., *The role of angiogenesis in tumor growth.* Seminars in cancer biology, 1992. **3**(2): p. 65-71.
4. Folkman, J., *Role of angiogenesis in tumor growth and metastasis.* Seminars in Oncology. **29**(6): p. 15-18.
5. Bischoff, J., *Cell adhesion and angiogenesis.* Journal of Clinical Investigation, 1997. **99**(3): p. 373-376.
6. Francavilla, C., L. Maddaluno, and U. Cavallaro, *The functional role of cell adhesion molecules in tumor angiogenesis.* Semin Cancer Biol, 2009. **19**(5): p. 298-309.
7. Avraamides, C.J., B. Garmy-Susini, and J.A. Varner, *Integrins in angiogenesis and lymphangiogenesis.* Nature reviews. Cancer, 2008. **8**(8): p. 604-617.
8. Barczyk, M., S. Carracedo, and D. Gullberg, *Integrins.* Cell and Tissue Research, 2010. **339**(1): p. 269-280.
9. Desgrosellier, J.S. and D.A. Cheresh, *Integrins in cancer: biological implications and therapeutic opportunities.* Nat Rev Cancer, 2010. **10**(1): p. 9-22.
10. Weis, S.M. and D.A. Cheresh, *αv Integrins in Angiogenesis and Cancer.* Cold Spring Harbor Perspectives in Medicine:, 2011. **1**(1): p. a006478.
11. Alphonso, A. and S.K. Alahari, *Stromal Cells and Integrins: Conforming to the Needs of the Tumor Microenvironment.* Neoplasia (New York, N.Y.), 2009. **11**(12): p. 1264-1271.
12. Watnick, R.S., *The Role of the Tumor Microenvironment in Regulating Angiogenesis.* Cold Spring Harbor Perspectives in Medicine, 2012. **2**(12): p. a006676.
13. Ostuni, R., et al., *Macrophages and cancer: from mechanisms to therapeutic implications.* Trends in immunology, 2015. **36**(4): p. 229-239.
14. Quail, D.F. and J.A. Joyce, *Microenvironmental regulation of tumor progression and metastasis.* Nature medicine, 2013. **19**(11): p. 1423-1437.
15. Hoshino, A., et al., *Tumour exosome integrins determine organotropic metastasis.* Nature, 2015. **527**(7578): p. 329-335.
16. Brooks, P.C., R.A. Clark, and D.A. Cheresh, *Requirement of vascular integrin alpha v beta 3 for angiogenesis.* Science, 1994. **264**(5158): p. 569-571.
17. Brooks, P.C., et al., *Integrin αvβ3 antagonists promote tumor regression by inducing apoptosis of angiogenic blood vessels.* Cell, 1994. **79**(7): p. 1157-1164.
18. Brooks, P., R. Clark, and D. Cheresh, *Requirement of vascular integrin alpha v beta 3 for angiogenesis.* Science, 1994. **264**(5158): p. 569-571.
19. Marelli, U.K., et al., *Tumor Targeting via Integrin Ligands.* Frontiers in Oncology, 2013. **3**(222).
20. Pierschbacher, M.D. and E. Ruoslahti, *Cell attachment activity of fibronectin can be duplicated by small synthetic fragments of the molecule.* Nature, 1984. **309**(5963): p. 30-33.
21. Kapp, T.G., et al., *A Comprehensive Evaluation of the Activity and Selectivity Profile of Ligands for RGD-binding Integrins.* Scientific Reports, 2017. **7**: p. 39805.
22. Haubner, R., et al., *Structural and Functional Aspects of RGD-Containing Cyclic Pentapeptides as Highly Potent and Selective Integrin αVβ3 Antagonists.* Journal of the American Chemical Society, 1996. **118**(32): p. 7461-7472.
23. Pasqualini, R., E. Koivunen, and E. Ruoslahti, *Alpha v integrins as receptors for tumor targeting by circulating ligands.* Nature biotechnology, 1997. **15**(6): p. 542-546.
24. Sugahara, K.N., et al., *Tumor-Penetrating iRGD Peptide Inhibits Metastasis.* Molecular cancer therapeutics, 2015. **14**(1): p. 120-128.
25. Mardilovich, A., et al., *Design of a Novel Fibronectin-Mimetic Peptide−Amphiphile for Functionalized Biomaterials.* Langmuir, 2006. **22**(7): p. 3259-3264.
26. Craig, J.A., et al., *Effect of linker and spacer on the design of a fibronectin-mimetic peptide evaluated via cell studies and AFM adhesion forces.* Langmuir, 2008. **24**(18): p. 10282-92.
27. Mitjans, F., et al., *An anti-alpha v-integrin antibody that blocks integrin function inhibits the development of a human melanoma in nude mice.* Journal of Cell Science, 1995. **108**(8): p. 2825.

28. Corti, A., et al., *The neovasculature homing motif NGR: more than meets the eye.* Blood, 2008. **112**(7): p. 2628-2635.
29. Binétruy-Tournaire, R., et al., *Identification of a peptide blocking vascular endothelial growth factor (VEGF)-mediated angiogenesis.* The EMBO Journal, 2000. **19**(7): p. 1525-1533.
30. Oku, N., et al., *Anti-neovascular therapy using novel peptides homing to angiogenic vessels.* Oncogene, 2002. **21**(17): p. 2662-9.
31. Nitta, S. and K. Numata, *Biopolymer-Based Nanoparticles for Drug/Gene Delivery and Tissue Engineering.* International Journal of Molecular Sciences, 2013. **14**(1): p. 1629-1654.
32. Boulaiz, H., et al., *Nanomedicine: Application Areas and Development Prospects.* International Journal of Molecular Sciences, 2011. **12**(5): p. 3303-3321.
33. Maeda, H., K. Tsukigawa, and J. Fang, *A Retrospective 30 Years After Discovery of the Enhanced Permeability and Retention Effect of Solid Tumors: Next-Generation Chemotherapeutics and Photodynamic Therapy—Problems, Solutions, and Prospects.* Microcirculation, 2016. **23**(3): p. 173-182.
34. Maeda, H., H. Nakamura, and J. Fang, *The EPR effect for macromolecular drug delivery to solid tumors: Improvement of tumor uptake, lowering of systemic toxicity, and distinct tumor imaging in vivo.* Advanced Drug Delivery Reviews, 2013. **65**(1): p. 71-79.
35. Maeda, H., G.Y. Bharate, and J. Daruwalla, *Polymeric drugs for efficient tumor-targeted drug delivery based on EPR-effect.* European Journal of Pharmaceutics and Biopharmaceutics, 2009. **71**(3): p. 409-419.
36. Allen, C., *Why I'm Holding onto Hope for Nano in Oncology.* Molecular Pharmaceutics, 2016. **13**(8): p. 2603-2604.
37. Huynh, E. and G. Zheng, *Cancer nanomedicine: addressing the dark side of the enhanced permeability and retention effect.* Nanomedicine, 2015. **10**(13): p. 1993-1995.
38. Nakamura, Y., et al., *Nanodrug Delivery: Is the Enhanced Permeability and Retention Effect Sufficient for Curing Cancer?* Bioconjugate Chemistry, 2016. **27**(10): p. 2225-2238.
39. Barz, M., *Complexity and simplification in the development of nanomedicines.* Nanomedicine, 2015. **10**(20): p. 3093-3097.
40. Arosio, D. and C. Casagrande, *Advancement in integrin facilitated drug delivery.* Advanced Drug Delivery Reviews, 2016. **97**: p. 111-143.
41. Ley, K., et al., *Integrin-based therapeutics: biological basis, clinical use and new drugs.* Nat Rev Drug Discov, 2016. **15**(3): p. 173-183.
42. E. Segal and R. Satchi-Fainaro, *Design and development of polymer conjugates as anti-angiogenic agents.* Advanced Drug Delivery Reviews, 2009. **61**(13): p. 1159-1176.
43. Pike, D.B. and H. Ghandehari, *HPMA copolymer–cyclic RGD conjugates for tumor targeting.* Advanced Drug Delivery Reviews, 2010. **62**(2): p. 167-183.
44. Ramsay, A.G., J.F. Marshall, and I.R. Hart, *Integrin trafficking and its role in cancer metastasis.* Cancer and Metastasis Reviews, 2007. **26**(3): p. 567.
45. Bradbury, M. *PET Imaging of Patients With Melanoma and Malignant Brain Tumors Using an 124I-labeled cRGDY Silica Nanomolecular Particle Tracer: A Microdosing Study [Internet]. Bethesda (MD): National Library of Medicine (US). 2000 - [cited 2017 Jan 5]. Available from:*. Available from: https://clinicaltrials.gov/ct2/show/NCT01266096?term=NCT01266096&rank=1 NLM identifier: NCT01266096.
46. Bradbury, M. *Targeted Silica Nanoparticles for Image-Guided Intraoperative Sentinel Lymph Node Mapping in Head and Neck Melanoma, Breast and Cervical/Uterine Cancer Patients. [Internet]. Bethesda (MD): National Library of Medicine (US). 2000 - [cited 2017 Jan 5]. Available from:*. Available from: https://ClinicalTrials.gov/show/NCT02106598 NLM Identifier: NCT02106598.
47. Phillips, E., et al., *Clinical translation of an ultrasmall inorganic optical-PET imaging nanoparticle probe.* Science Translational Medicine, 2014. **6**(260): p. 260ra149-260ra149.
48. Line, B.R., et al., *Targeting tumor angiogenesis: comparison of peptide and polymer-peptide conjugates.* Journal of Nuclear Medicine, 2005. **46**(9): p. 1552-1560.
49. Mitra, A., et al., *Targeting tumor angiogenic vasculature using polymer–RGD conjugates.* Journal of Controlled Release, 2005. **102**(1): p. 191-201.

50. Kunjachan, S., et al., *Passive versus active tumor targeting using RGD-and NGR-modified polymeric nanomedicines.* Nano letters, 2014. **14**(2): p. 972-981.
51. Mitra, A., et al., *Polymeric conjugates of mono- and bi-cyclic αVβ3 binding peptides for tumor targeting.* Journal of Controlled Release, 2006. **114**(2): p. 175-183.
52. Gormley, A.J., et al., *Biological evaluation of RGDfK-gold nanorod conjugates for prostate cancer treatment.* Journal of Drug Targeting, 2011. **19**(10): p. 915-924.
53. Allen, T.M., *Ligand-targeted therapeutics in anticancer therapy.* Nat Rev Cancer, 2002. **2**(10): p. 750-763.
54. Wang, F., et al., *The Functions and Applications of RGD in Tumor Therapy and Tissue Engineering.* International Journal of Molecular Sciences, 2013. **14**(7): p. 13447-13462.
55. M. J. Vicent and R. Duncan, *Polymer conjugates: nanosized medicines for treating cancer.* Trends Biotechnol, 2006. **24**(1): p. 39-47.
56. Kawasaki, K., et al., *Amino acids and peptides. XIV. Laminin related peptides and their inhibitory effect on experimental metastasis formation.* Biochemical and Biophysical Research Communications, 1991. **174**(3): p. 1159-1162.
57. Kawasaki, K., et al., *Preparation of (Mrg-Gly-Asp)-(amino-poly (ethylene glycol)) hybrids and their inhibitory effect on experimental metastasis.* Chemical and pharmaceutical bulletin, 1991. **39**(12): p. 3373-3375.
58. Yamamoto, Y., Y. Tsutsumi, and T. Mayumi, *Molecular design of bioconjugated cell adhesion peptide with a water-soluble polymeric modifier for enhancement of antimetastatic effect.* Current drug targets, 2002. **3**(2): p. 123-130.
59. Saiki, I., et al., *Antimetastatic activity of polymeric RGDT peptides conjugated with poly (ethylene glycol).* Japanese journal of cancer research, 1993. **84**(5): p. 558-565.
60. Komazawa, H., et al., *Inhibition of tumor metastasis by a synthetic polymer containing a cell-adhesive RGDS peptide.* Journal of bioactive and compatible polymers, 1993. **8**(3): p. 258-274.
61. Komazawa, H., et al., *Synthetic Arg-Gly-Asp-Ser analogues of the cell recognition site of fibronectin that retain antimetastatic and anti-cell adhesive properties.* Biological and Pharmaceutical Bulletin, 1993. **16**(10): p. 997-1003.
62. Komazawa, H., et al., *Inhibition of tumor metastasis by Arg-Gly-Asp-Ser (RGDS) peptide conjugated with sulfated chitin derivative, SCM-chitin-RGDS.* Clinical & experimental metastasis, 1993. **11**(6): p. 482-491.
63. Komazawa, H., et al., *The conjugation of RGDS peptide with CM-chitin augments the peptide-mediated inhibition of tumor metastasis.* Carbohydrate polymers, 1993. **21**(4): p. 299-307.
64. Polyak, D., et al., *Development of PEGylated doxorubicin-E-[c(RGDfK)2] conjugate for integrin-targeted cancer therapy.* Polymers for Advanced Technologies, 2011. **22**(1): p. 103-113.
65. Eldar-Boock, A., et al., *Integrin-assisted drug delivery of nano-scaled polymer therapeutics bearing paclitaxel.* Biomaterials, 2011. **32**(15): p. 3862-74.
66. K.-W. Wan, M.J.V., , R. Duncan. *Targeting endothelial cells using HPMA copolymer-doxorubicin-RGD conjugates*. *Int. Symp. Control. Release Bioact. Mater* 2003.
67. Ray, A., et al., *Comparison of Active and Passive Targeting of Docetaxel for Prostate Cancer Therapy by HPMA Copolymer–RGDfK Conjugates.* Molecular Pharmaceutics, 2011. **8**(4): p. 1090-1099.
68. Borgman, M.P., et al., *Targetable HPMA Copolymer–Aminohexylgeldanamycin Conjugates for Prostate Cancer Therapy.* Pharmaceutical research, 2009. **26**(6): p. 1407-1418.
69. M. P. Borgman, et al., *Biodistribution of HPMA copolymer-aminohexylgeldanamycin-RGDfK conjugates for prostate cancer drug delivery.* Mol Pharm, 2009. **6**(6): p. 1836-47.
70. Greish, K., et al., *Anticancer and antiangiogenic activity of HPMA copolymer-aminohexylgeldanamycin-RGDfK conjugates for prostate cancer therapy.* Journal of Controlled Release, 2011. **151**(3): p. 263-270.
71. Shukla, R., et al., *Tumor angiogenic vasculature targeting with PAMAM dendrimer–RGD conjugates.* Chemical communications, 2005(46): p. 5739-5741.
72. Zhu, S., et al., *Partly PEGylated polyamidoamine dendrimer for tumor-selective targeting of doxorubicin: the effects of PEGylation degree and drug conjugation style.* Biomaterials, 2010. **31**(6): p. 1360-1371.

73. Zhu, S., et al., *PEGylated PAMAM Dendrimer-Doxorubicin Conjugates: In Vitro Evaluation and In Vivo Tumor Accumulation.* Pharmaceutical Research, 2010. **27**(1): p. 161-174.
74. Zhu, S., et al., *RGD-Modified PEG-PAMAM-DOX Conjugate: In Vitro and In Vivo Targeting to Both Tumor Neovascular Endothelial Cells and Tumor Cells.* Advanced Materials, 2011. **23**(12): p. H84-H89.
75. Zhang, L., et al., *RGD-modified PEG–PAMAM–DOX conjugates: In vitro and in vivo studies for glioma.* European Journal of Pharmaceutics and Biopharmaceutics, 2011. **79**(2): p. 232-240.
76. Wang, K., et al., *Tumor penetrability and anti-angiogenesis using iRGD-mediated delivery of doxorubicin-polymer conjugates.* Biomaterials, 2014. **35**(30): p. 8735-8747.
77. Wang, K., et al., *Development of biodegradable polymeric implants of RGD-modified PEG-PAMAM-DOX conjugates for long-term intratumoral release.* Drug delivery, 2015. **22**(3): p. 389-399.
78. Zhang, X., et al., *Tumor tropic delivery of doxorubicin-polymer conjugates using mesenchymal stem cells for glioma therapy.* Biomaterials, 2015. **39**: p. 269-281.
79. Xu, X.-D., et al., *Smart and hyper-fast responsive polyprodrug nanoplatform for targeted cancer therapy.* Biomaterials, 2016. **76**: p. 238-249.
80. Brinkhuis, R.P., F.P.J.T. Rutjes, and J.C.M. van Hest, *Polymeric vesicles in biomedical applications.* Polymer Chemistry, 2011. **2**(7): p. 1449-1462.
81. Yang, J., et al., *Targeted delivery of the RGD-labeled biodegradable polymersomes loaded with the hydrophilic drug oxymatrine on cultured hepatic stellate cells and liver fibrosis in rats.* European Journal of Pharmaceutical Sciences, 2014. **52**: p. 180-190.
82. Simón-Gracia, L., et al., *iRGD peptide conjugation potentiates intraperitoneal tumor delivery of paclitaxel with polymersomes.* Biomaterials, 2016. **104**: p. 247-257.
83. Chen, Y., et al., *Dual-functional c (RGDyK)-decorated Pluronic micelles designed for antiangiogenesis and the treatment of drug-resistant tumor.* International journal of nanomedicine, 2015. **10**: p. 4863.
84. Huang, Y., et al., *c (RGDyK)-decorated Pluronic micelles for enhanced doxorubicin and paclitaxel delivery to brain glioma.* International journal of nanomedicine, 2016. **11**: p. 1629.
85. Chen, Y., et al., *In Vivo Biodistribution and Anti-Tumor Efficacy Evaluation of Doxorubicin and Paclitaxel-Loaded Pluronic Micelles Decorated with c (RGDyK) Peptide.* PloS one, 2016. **11**(3): p. e0149952.
86. Hu, Z., et al., *Arg-Gly-Asp (RGD) peptide conjugated poly (lactic acid)–poly (ethylene oxide) micelle for targeted drug delivery.* Journal of Biomedical Materials Research Part A, 2008. **85**(3): p. 797-807.
87. Gao, Y., et al., *Enhanced antitumor efficacy by cyclic RGDyK-conjugated and paclitaxel-loaded pH-responsive polymeric micelles.* Acta biomaterialia, 2015. **23**: p. 127-135.
88. Zhan, C., et al., *Cyclic RGD conjugated poly(ethylene glycol)-co-poly(lactic acid) micelle enhances paclitaxel anti-glioblastoma effect.* Journal of Controlled Release, 2010. **143**(1): p. 136-142.
89. Li, A.J., et al., *Efficient delivery of docetaxel for the treatment of brain tumors by cyclic RGD-tagged polymeric micelles.* Molecular medicine reports, 2015. **11**(4): p. 3078-3086.
90. Zhao, L., et al., *Development of RGD-functionalized PEG-PLA micelles for delivery of curcumin.* Journal of biomedical nanotechnology, 2015. **11**(3): p. 436-446.
91. Xiong, X.-B., et al., *The therapeutic response to multifunctional polymeric nano-conjugates in the targeted cellular and subcellular delivery of doxorubicin.* Biomaterials, 2010. **31**(4): p. 757-768.
92. Makino, J., et al., *CRGD-installed polymeric micelles loading platinum anticancer drugs enable cooperative treatment against lymph node metastasis.* Journal of Controlled Release, 2015. **220**: p. 783-791.
93. Miura, Y., et al., *Cyclic RGD-linked polymeric micelles for targeted delivery of platinum anticancer drugs to glioblastoma through the blood–brain tumor barrier.* ACS nano, 2013. **7**(10): p. 8583-8592.
94. Song, W., et al., *Methoxypoly(ethylene glycol)-block-Poly(L-glutamic acid)-Loaded Cisplatin and a Combination With iRGD for the Treatment of Non-Small-Cell Lung Cancers.* Macromolecular Bioscience, 2012. **12**(11): p. 1514-1523.

95. Guan, X., et al., *Highly efficient drug delivery polymeric micelles with charge-switching and cyclic rgd targeting for treatment of glioblastoma*. Digest Journal of Nanomaterials & Biostructures (DJNB), 2015. **10**(3).
96. Guan, X., et al., *Target Delivery of Daunorubicin to Glioblastoma by Cyclic RGD-Linked PEG-PLA Micelles.* Journal of Macromolecular Science, Part A, 2015. **52**(5): p. 401-406.
97. Guan, X., et al., *Cyclic RGD targeting nanoparticles with pH sensitive polymer-drug conjugates for effective treatment of melanoma.* RSC Advances, 2014. **4**(98): p. 55187-55194.
98. Pan, G., et al., *Esterase-responsive polymeric prodrug-based tumor targeting nanoparticles for improved anti-tumor performance against colon cancer.* RSC Advances, 2016. **6**(48): p. 42109-42119.
99. Temming, K., et al., *Evaluation of RGD-Targeted Albumin Carriers for Specific Delivery of Auristatin E to Tumor Blood Vessels*. Bioconjugate Chemistry, 2006. **17**(6): p. 1385-1394.
100. Temming, K., et al., *Improved Efficacy of αvβ3-Targeted Albumin Conjugates by Conjugation of a Novel Auristatin Derivative.* Molecular Pharmaceutics, 2007. **4**(5): p. 686-694.
101. Ji, S., et al., *RGD-conjugated albumin nanoparticles as a novel delivery vehicle in pancreatic cancer therapy.* Cancer biology & therapy, 2012. **13**(4): p. 206-215.
102. Oberstein, P.E. and K.P. Olive, *Pancreatic cancer: why is it so hard to treat?* Therapeutic Advances in Gastroenterology, 2013. **6**(4): p. 321-337.
103. Graf, N., et al., *αVβ3 integrin-targeted PLGA-PEG nanoparticles for enhanced anti-tumor efficacy of a Pt (IV) prodrug.* ACS nano, 2012. **6**(5): p. 4530-4539.
104. Zhu, Z., et al., *The effect of hydrophilic chain length and iRGD on drug delivery from poly(ε-caprolactone)-poly(N-vinylpyrrolidone) nanoparticles.* Biomaterials, 2011. **32**(35): p. 9525-9535.
105. Zhang, L., et al., *RGD-peptide conjugated inulin-ibuprofen nanoparticles for targeted delivery of Epirubicin.* Colloids and Surfaces B: Biointerfaces, 2016. **144**: p. 81-89.
106. Qiu, L., et al., *cRGDyK modified pH responsive nanoparticles for specific intracellular delivery of doxorubicin.* Acta Biomaterialia, 2016. **30**: p. 285-298.
107. Guo, Y., et al., *RGD-decorated redox-responsive d-α-tocopherol polyethylene glycol succinate–poly (lactide) nanoparticles for targeted drug delivery*. Journal of Materials Chemistry B, 2016. **4**(13): p. 2338-2350.
108. Noble, G.T., et al., *Ligand-targeted liposome design: challenges and fundamental considerations.* Trends in Biotechnology. **32**(1): p. 32-45.
109. Schiffelers, R.M., et al., *Anti-tumor efficacy of tumor vasculature-targeted liposomal doxorubicin.* Journal of Controlled Release, 2003. **91**(1–2): p. 115-122.
110. Xiong, X.B., et al., *Enhanced intracellular delivery and improved antitumor efficacy of doxorubicin by sterically stabilized liposomes modified with a synthetic RGD mimetic.* J Control Release, 2005. **107**(2): p. 262-75.
111. Xiong, X.B., et al., *Intracellular delivery of doxorubicin with RGD-modified sterically stabilized liposomes for an improved antitumor efficacy: in vitro and in vivo.* J Pharm Sci, 2005. **94**(8): p. 1782-93.
112. Zhao, H., et al., *RGD-based strategies for improving antitumor activity of paclitaxel-loaded liposomes in nude mice xenografted with human ovarian cancer.* J Drug Target, 2009. **17**(1): p. 10-8.
113. Dai, W., et al., *Peptide PHSCNK as an integrin alpha5beta1 antagonist targets stealth liposomes to integrin-overexpressing melanoma*. Nanomedicine, 2012. **8**(7): p. 1152-61.
114. Dai, W., et al., *PHSCNK-Modified and doxorubicin-loaded liposomes as a dual targeting system to integrin-overexpressing tumor neovasculature and tumor cells.* J Drug Target, 2010. **18**(4): p. 254-63.
115. Khalili, P., et al., *A non-RGD-based integrin binding peptide (ATN-161) blocks breast cancer growth and metastasis in vivo.* Mol Cancer Ther, 2006. **5**(9): p. 2271-80.
116. Yao, N., et al., *Discovery of Targeting Ligands for Breast Cancer Cells Using the One-Bead One-Compound Combinatorial Method.* Journal of Medicinal Chemistry, 2009. **52**(1): p. 126-133.
117. Yao, N., et al., *Structure −Activity Relationship Studies of Targeting Ligands against Breast Cancer Cells.* Journal of Medicinal Chemistry, 2009. **52**(21): p. 6744-6751.

118. Dai, W., et al., *Combined mTOR inhibitor rapamycin and doxorubicin-loaded cyclic octapeptide modified liposomes for targeting integrin α3 in triple-negative breast cancer.* Biomaterials, 2014. **35**(20): p. 5347-5358.
119. Cao, Y., et al., *Anti-tumor effect of RGD modified PTX loaded liposome on prostatic cancer.* International Journal of Clinical and Experimental Medicine, 2015. **8**(8): p. 12182-12191.
120. Scherzinger-Laude, K., et al., *Treatment of neuroblastoma and rhabdomyosarcoma using RGD-modified liposomal formulations of patupilone (EPO906).* Int J Nanomedicine, 2013. **8**: p. 2197-211.
121. Lopez-Cebral, R., et al., *Application of NMR spectroscopy in the development of a biomimetic approach for hydrophobic drug association with physical hydrogels.* Colloids and Surfaces B-Biointerfaces, 2014. **115**: p. 391-399.
122. Ji, T., et al., *An MMP-2 Responsive Liposome Integrating Antifibrosis and Chemotherapeutic Drugs for Enhanced Drug Perfusion and Efficacy in Pancreatic Cancer.* ACS Appl Mater Interfaces, 2016. **8**(5): p. 3438-45.
123. Du, H., et al., *Novel tetrapeptide, RGDF, mediated tumor specific liposomal doxorubicin (DOX) preparations.* Mol Pharm, 2011. **8**(4): p. 1224-32.
124. Li, Y., et al., *RGD-fatty alcohol-modified docetaxel liposomes improve tumor selectivity in vivo.* International Journal of Pharmaceutics, 2014. **468**(1–2): p. 133-141.
125. Chang, M., et al., *RGD-modified pH-sensitive liposomes for docetaxel tumor targeting.* Colloids and Surfaces B: Biointerfaces, 2015. **129**: p. 175-182.
126. Zhang, Q., et al., *Dual-functionalized liposomal delivery system for solid tumors based on RGD and a pH-responsive antimicrobial peptide.* Scientific Reports, 2016. **6**: p. 19800.
127. Liang, B., et al., *Integrinβ6-Targeted Immunoliposomes Mediate Tumor-Specific Drug Delivery and Enhance Therapeutic Efficacy in Colon Carcinoma.* Clinical Cancer Research, 2015. **21**(5): p. 1183.
128. Bao, Y., et al., *A safe, simple and efficient doxorubicin prodrug hybrid micelle for overcoming tumor multidrug resistance and targeting delivery.* Journal of Controlled Release, 2016. **235**: p. 182-194.
129. Saraf, P., et al., *In vitro and in vivo efficacy of self-assembling RGD peptide amphiphiles for targeted delivery of paclitaxel.* Pharmaceutical research, 2015. **32**(9): p. 3087-3101.
130. Raj, A., et al., *Binding and uptake of novel RGD micelles to the αvβ3 integrin receptor for targeted drug delivery.* Journal of Drug Targeting, 2014. **22**(6): p. 518-527.
131. Shi, K., et al., *Arginine-glycine-aspartic acid-modified lipid-polymer hybrid nanoparticles for docetaxel delivery in glioblastoma multiforme.* Journal of biomedical nanotechnology, 2015. **11**(3): p. 382-391.
132. Agrawal, U., et al., *Tailored polymer–lipid hybrid nanoparticles for the delivery of drug conjugate: Dual strategy for brain targeting.* Colloids and Surfaces B: Biointerfaces, 2015. **126**: p. 414-425.
133. Hu, J.-J., D. Xiao, and X.-Z. Zhang, *Advances in Peptide Functionalization on Mesoporous Silica Nanoparticles for Controlled Drug Release.* Small, 2016. **12**(25): p. 3344-3359.
134. Chen, Y., et al., *Multifunctional mesoporous silica nanocarriers for stimuli-responsive target delivery of anticancer drugs.* RSC Advances, 2016. **6**(94): p. 92073-92091.
135. Yang, Y. and C. Yu, *Advances in silica based nanoparticles for targeted cancer therapy.* Nanomedicine: Nanotechnology, Biology and Medicine, 2016. **12**(2): p. 317-332.
136. Murugan, C., et al., *Combinatorial nanocarrier based drug delivery approach for amalgamation of anti-tumor agents in breast cancer cells: an improved nanomedicine strategy.* Sci. Rep., 2016. **6**, p. 34053.
137. Xiao, D., et al., *A redox-responsive mesoporous silica nanoparticle with a therapeutic peptide shell for tumor targeting synergistic therapy.* Nanoscale, 2016. **8**(37): p. 16702-16709.
138. Zhao, N., et al., *RGD-conjugated mesoporous silica-encapsulated gold nanorods enhance the sensitization of triple-negative breast cancer to megavoltage radiation therapy.* International Journal of Nanomedicine, 2016. **11**: p. 5595-5610.
139. Wu, X., et al., *Targeted Mesoporous Silica Nanoparticles Delivering Arsenic Trioxide with Environment Sensitive Drug Release for Effective Treatment of Triple Negative Breast Cancer.* ACS Biomaterials Science & Engineering, 2016. **2**(4): p. 501-507.

140. Yeh, I.C., et al., *Integrin Targeted Gold Nanoparticles Potentiate Cancer Radiation Sensitivity: Synthesizing and modifying gold nanorods to target cancer cells.* IEEE Nanotechnology Magazine, 2016. **10**(1): p. 4-15.
141. Fung, A.S., et al., *The effect of chemotherapeutic agents on tumor vasculature in subcutaneous and orthotopic human tumor xenografts.* BMC Cancer, 2015. **15**: p. 112.
142. Nayerossadat, N., T. Maedeh, and P.A. Ali, *Viral and nonviral delivery systems for gene delivery.* Advanced Biomedical Research, 2012. **1**: p. 27.
143. Aoki, Y., et al., *Potential tumor-targeting peptide vector of histidylated oligolysine conjugated to a tumor-homing RGD motif.* Cancer gene therapy, 2001. **8**(10): p.783-787.
144. Cao, D., et al., *Nanocomplexes from RGD-modified generation 1.0 polyamidoamine based copolymers used for intravascular gene release to prevent restenosis.* Nanomedicine, 2016. **11**(4): p. 359-375.
145. Schiffelers, R.M., et al., *Cancer siRNA therapy by tumor selective delivery with ligand-targeted sterically stabilized nanoparticle.* Nucleic acids research, 2004. **32**(19): p. e149-e149.
146. Kim, W.J., et al., *Soluble Flt-1 gene delivery using PEI-g-PEG-RGD conjugate for anti-angiogenesis.* Journal of Controlled Release, 2005. **106**(1): p. 224-234.
147. Kim, W.J., et al., *Anti-angiogenic inhibition of tumor growth by systemic delivery of PEI-g-PEG-RGD/pCMV-sFlt-1 complexes in tumor-bearing mice.* Journal of controlled release, 2006. **114**(3): p. 381-388.
148. Kim, J., S.W. Kim, and W.J. Kim, *PEI-g-PEG-RGD/small interference RNA polyplex-mediated silencing of vascular endothelial growth factor receptor and its potential as an anti-angiogenic tumor therapeutic strategy.* Oligonucleotides, 2011. **21**(2): p. 101-107.
149. Wang, W., et al., *RGD Peptides-Conjugated Pluronic Triblock Copolymers Encapsulated with AP-2α Expression Plasmid for Targeting Gastric Cancer Therapy in Vitro and in Vivo.* International Journal of Molecular Sciences, 2015. **16**(7): p. 16263–16274.
150. Garg, S.M., et al., *Polymeric micelles for MCL-1 gene silencing in breast tumors following systemic administration.* Nanomedicine, 2016. **11**(17): p. 2319-2339.
151. Scheinman, R.I., et al., *Functionalized STAT1 siRNA nanoparticles regress rheumatoid arthritis in a mouse model.* Nanomedicine, 2011. **6**(10): p. 1669-1682.
152. Shen, J., et al., *iRGD Conjugated TPGS Mediates Codelivery of Paclitaxel and Survivin shRNA for the Reversal of Lung Cancer Resistance.* Molecular Pharmaceutics, 2014. **11**(8): p. 2579-2591.
153. Balazs, D.A. and W. Godbey, *Liposomes for Use in Gene Delivery.* Journal of Drug Delivery, 2011. 2011: p. 326497.
154. Hood, J.D., et al., *Tumor regression by targeted gene delivery to the neovasculature.* Science, 2002. **296**(5577): p. 2404-7.
155. Majumder, P., et al., *Inhibiting tumor growth by targeting liposomally encapsulated CDC20siRNA to tumor vasculature: therapeutic RNA interference.* J Control Release, 2014. **180**: p. 100-8.
156. Majumder, P. and A. Chaudhuri, *Integrin-Mediated Targeting of Liposomally Bound siRNAs to Tumor Vasculatures*. Humana Press: Totowa, NJ. p. 1-24.
157. Hamada, K., et al., *Increased expression of the genes for mitotic spindle assembly and chromosome segregation in both lung and pancreatic carcinomas.* Cancer Genomics-Proteomics, 2004. **1**(3): p. 231-240.
158. Rengaswamy, V., et al., *RGD liposome-protamine-siRNA (LPR) nanoparticles targeting PAX3-FOXO1 for alveolar rhabdomyosarcoma therapy.* J Control Release, 2016. **235**: p. 319-27.
159. Chen, H., et al., *F-19 NMR: a valuable tool for studying biological events.* Chemical Society Reviews, 2013. **42**(20): p. 7971-7982.
160. Sato, Y., et al., *A pH-sensitive cationic lipid facilitates the delivery of liposomal siRNA and gene silencing activity in vitro and in vivo.* Journal of Controlled Release, 2012. **163**(3): p. 267-276.
161. Sakurai, Y., et al., *RNAi-mediated gene knockdown and anti-angiogenic therapy of RCCs using a cyclic RGD-modified liposomal-siRNA system.* Journal of Controlled Release, 2014. **173**: p. 110-118.
162. Adil, M., et al., *PR_b functionalized stealth liposomes for targeted delivery to metastatic colon cancer.* Biomaterials Science, 2013. **1**(4): p. 393-401.

163. Song, L., et al., *Tumor specific delivery and therapy mediate by integrin β6-target immunoliposomes for β6-siRNA in colon carcinoma*. 2016. **7**: p. 85163-85175.
164. Zhang, P., et al., *Near Infrared-Guided Smart Nanocarriers for MicroRNA-Controlled Release of Doxorubicin/siRNA with Intracellular ATP as Fuel.* ACS Nano, 2016. **10**(3): p. 3637-3647.
165. Yi, Y., et al., *Targeted systemic delivery of siRNA to cervical cancer model using cyclic RGD-installed unimer polyion complex-assembled gold nanoparticles.* Journal of Controlled Release, 2016. **244, Part B**: p. 247-256.
166. M. Lee, et al., *Rapid Pharmacokinetic and Biodistribution Studies Using Cholorotoxin-Conjugated Iron Oxide Nanoparticles: A Novel Non-Radioactive Method.* PLoS One, 2010. **5**(3): p. e9536.
167. P. A. Vasey, et al., *Phase I clinical and pharmacokinetic study of PK1 [N-(2-hydroxypropyl)methacrylamide copolymer doxorubicin]: first member of a new class of chemotherapeutic agents-drug-polymer conjugates. Cancer Research Campaign Phase I/II Committee.* Clin Cancer Res, 1999. **5**(1): p. 83-94.
168. M. Baker, *Whole-animal imaging: The whole picture.* Nature, 2010. **463**(7283): p. 977-80.
169. M. M. Herth, et al., *Radioactive labeling of defined HPMA-based polymeric structures using [18F]FETos for in vivo imaging by positron emission tomography.* Biomacromolecules, 2009. **10**(7): p. 1697-703.
170. M. M. Herth, et al., *72/74As-labeling of HPMA based polymers for long-term in vivo PET imaging.* Bioorg Med Chem Lett, 2010. **20**(18): p. 5454-8.
171. M. Longmire, P. L. Choyke, and H. Kobayashi, *Dendrimer-based contrast agents for molecular imaging.* Curr Top Med Chem, 2008. **8**(14): p. 1180-6.
172. S.C. Richardson, et al., *The use of fluorescence microscopy to define polymer localisation to the late endocytic compartments in cells that are targets for drug delivery.* J Control Release, 2008. **127**(1): p. 1-11.
173. X. Chen, P. S. Conti, and R. A. Moats, *In vivo near-infrared fluorescence imaging of integrin alphavbeta3 in brain tumor xenografts.* Cancer Res, 2004. **64**(21): p. 8009-14.
174. S. Bhaskar, et al., *Multifunctional Nanocarriers for diagnostics, drug delivery and targeted treatment across blood-brain barrier: perspectives on tracking and neuroimaging.* Part Fibre Toxicol, 2010. **7**(3).
175. R. Gaspar and R. Duncan, *Nanomedicine(s) under the microscope.* Mol Pharm, 2011. **8**(6): p. 2101-41.
176. M. P. Melancon, R. J. Stafford, and C. Li, *Challenges to effective cancer nanotheranostics.* J Control Release, 2012. **164**(2): p. 177-82.
177. M. E. Gindy and R. K. Prud'homme, *Multifunctional nanoparticles for imaging, delivery and targeting in cancer therapy.* Expert Opin Drug Deliv, 2009. **6**(8): p. 865-78.
178. Yao, V.J., et al., *Ligand-targeted theranostic nanomedicines against cancer.* Journal of Controlled Release, 2016. **240**: p. 267-286.
179. Falagan-Lotsch, P., E.M. Grzincic, and C.J. Murphy, *New Advances in Nanotechnology-Based Diagnosis and Therapeutics for Breast Cancer: An Assessment of Active-Targeting Inorganic Nanoplatforms.* Bioconjugate Chemistry, 2017. **28**(1): p 135-152.
180. Arranja, A.G., et al., *Tumor-targeted nanomedicines for cancer theranostics.* Pharmacological Research, 2017. **115**: p. 87-95.
181. Thakor, A.S., et al., *Clinically Approved Nanoparticle Imaging Agents.* Journal of Nuclear Medicine, 2016. **57**(12): p. 1833-1837.
182. Anselmo, A.C. and S. Mitragotri, *Nanoparticles in the clinic.* Bioengineering & Translational Medicine, 2016. **1**(1): p. 10-29.
183. Chen, X., et al., *MicroPET imaging of brain tumor angiogenesis with 18F-labeled PEGylated RGD peptide.* European Journal of Nuclear Medicine and Molecular Imaging, 2004. **31**(8): p. 1081-1089.
184. Chen, X., et al., *Pharmacokinetics and tumor retention of ^{125}I-labeled RGD peptide are improved by PEGylation.* Nuclear Medicine and Biology, 2004. **31**(1): p. 11-19.
185. Chen, K., J. Xie, and X. Chen, *RGD-Human Serum Albumin Conjugates as Efficient Tumor Targeting Probes.* Molecular Imaging, 2009. **8**(2): p. 65-73.

186. Ma, Y., et al., *18F labeled RGD-A7R peptide for dual integrin and VEGF-targeted tumor imaging in mice bearing U87MG tumors.* Journal of Labelled Compounds and Radiopharmaceuticals, 2014. **57**(11): p. 627-631.
187. Ma, Y., et al., *18F-radiolabeled RGD-A7R-conjugated nano-particles for integrin and VEGF-targeted tumor imaging.* Journal of Radioanalytical and Nuclear Chemistry, 2016. **308**(2): p. 741-746.
188. Ke, T., et al., *RGD targeted poly(L-glutamic acid)-cystamine-(Gd-DO3A) conjugate for detecting angiogenesis biomarker α(v)β(3) integrin with MR T(1) mapping.* International Journal of Nanomedicine, 2007. **2**(2): p. 191-199.
189. Zarabi, B., et al., *Noninvasive Monitoring of HPMA Copolymer–RGDfK Conjugates by Magnetic Resonance Imaging.* Pharmaceutical Research, 2009. **26**(5): p. 1121-1129.
190. Borgman, M.P., et al., *Tumor-Targeted HPMA Copolymer-(RGDfK)-(CHX-A"-DTPA) Conjugates Show Increased Kidney Accumulation.* Journal of controlled release : official journal of the Controlled Release Society, 2008. **132**(3): p. 193-199.
191. Mitra, A., et al., *Polymer-peptide conjugates for angiogenesis targeted tumor radiotherapy.* Nuclear Medicine and Biology. **33**(1): p. 43-52.
192. Mitra, A., et al., *Technetium-99m-Labeled N-(2-hydroxypropyl) methacrylamide copolymers: synthesis, characterization, and in vivo biodistribution.* Pharmaceutical research, 2004. **21**(7): p. 1153-1159.
193. Yuan, J., et al., *Synthesis and characterization of theranostic poly (HPMA)-c (RGDyK)-DOTA-64Cu copolymer targeting tumor angiogenesis: tumor localization visualized by positron emission tomography.* Mol Imaging, 2013. **12**(3): p. 1-10.
194. Boswell, C.A., et al., *Synthesis, Characterization, and Biological Evaluation of Integrin αvβ3-Targeted PAMAM Dendrimers.* Molecular Pharmaceutics, 2008. **5**(4): p. 527-539.
195. Li, Q., et al., *RGD conjugated, Cy5. 5 labeled polyamidoamine dendrimers for targeted near-infrared fluorescence imaging of esophageal squamous cell carcinoma.* RSC Advances, 2016. **6**(78): p. 74560-74566.
196. Sun, L., et al., *Stimuli-Responsive Biodegradable Hyperbranched Polymer–Gadolinium Conjugates as Efficient and Biocompatible Nanoscale Magnetic Resonance Imaging Contrast Agents.* ACS applied materials & interfaces, 2016. **8**(16): p. 10499-10512.
197. Kawamura, W., et al., *Density-tunable conjugation of cyclic RGD ligands with polyion complex vesicles for the neovascular imaging of orthotopic glioblastomas.* Science and Technology of Advanced Materials, 2016. **16**(3) p. 35004.
198. Guan, X., et al., *Cyclic RGD targeting cisplatin micelles for near-infrared imaging-guided chemotherapy.* RSC Advances, 2016. **6**(2): p. 1151-1157.
199. Sipkins, D.A., et al., *Detection of tumor angiogenesis in vivo by [alpha]v[beta]3-targeted magnetic resonance imaging.* Nat Med, 1998. **4**(5): p. 623-626.
200. Kluza, E., et al., *Synergistic targeting of alphavbeta3 integrin and galectin-1 with heteromultivalent paramagnetic liposomes for combined MR imaging and treatment of angiogenesis.* Nano Lett, 2010. **10**(1): p. 52-8.
201. Macchioni, A., et al., *Determining accurate molecular sizes in solution through NMR diffusion spectroscopy.* Chemical Society Reviews, 2008. **37**(3): p. 479-489.
202. Thijssen, V.L.J.L., et al., *Galectin-1 is essential in tumor angiogenesis and is a target for antiangiogenesis therapy.* Proceedings of the National Academy of Sciences of the United States of America, 2006. **103**(43): p. 15975-15980.
203. Ohno, A., et al., *In-Cell NMR Spectroscopy in Protein Chemistry and Drug Discovery.* Current Topics in Medicinal Chemistry, 2011. **11**(1): p. 68-73.
204. Rangger, C., et al., *Influence of PEGylation and RGD loading on the targeting properties of radiolabeled liposomal nanoparticles.* International Journal of Nanomedicine, 2012. **7**: p. 5889-5900.
205. Sonali, et al., *RGD-TPGS decorated theranostic liposomes for brain targeted delivery.* Colloids and Surfaces B: Biointerfaces, 2016. **147**: p. 129-141.
206. Yu, M.K., J. Park, and S. Jon, *Targeting Strategies for Multifunctional Nanoparticles in Cancer Imaging and Therapy.* Theranostics, 2012. **2**(1): p. 3-44.

207. Swierczewska, M., S. Lee, and X. Chen, *Inorganic Nanoparticles for Multimodal Molecular Imaging.* Molecular imaging, 2011. **10**(1): p. 3-16.
208. Zhang, C., et al., *Specific Targeting of Tumor Angiogenesis by RGD-Conjugated Ultrasmall Superparamagnetic Iron Oxide Particles Using a Clinical 1.5-T Magnetic Resonance Scanner.* Cancer Research, 2007. **67**(4): p. 1555-1562.
209. Liu, Y., Y. Yang, and C. Zhang, *A concise review of magnetic resonance molecular imaging of tumor angiogenesis by targeting integrin αvβ3 with magnetic probes.* International Journal of Nanomedicine, 2013. **8**: p. 1083-1093.
210. Chen, H., et al., *Clinical Application of Radiolabeled RGD Peptides for PET Imaging of Integrin α(v)β(3).* Theranostics, 2016. **6**(1): p. 78-92.
211. Danhier, F., A.L. Breton, and V. Préat, *RGD-Based Strategies To Target Alpha(v) Beta(3) Integrin in Cancer Therapy and Diagnosis.* Molecular Pharmaceutics, 2012. **9**(11): p. 2961-2973.
212. Ow, H., et al., *Bright and Stable Core−Shell Fluorescent Silica Nanoparticles.* Nano Letters, 2005. **5**(1): p. 113-117.
213. Kazmierczak, P.M., et al., *αvβ3-Integrin–Targeted Magnetic Resonance Imaging for the Assessment of Early Antiangiogenic Therapy Effects in Orthotopic Breast Cancer Xenografts.* Investigative Radiology, 2016. **51**(11): p. 746-755.
214. Luo, Y., et al., *RGD-functionalized ultrasmall iron oxide nanoparticles for targeted T1-weighted MR imaging of gliomas.* Nanoscale, 2015. **7**(34): p. 14538-14546.
215. Zhang, J., et al., *Dual-targeting superparamagnetic iron oxide nanoprobes with high and low target density for brain glioma imaging.* Journal of Colloid and Interface Science, 2016. **469**: p. 86-92.
216. Richard, S., et al., *Iron oxide nanoparticle surface decorated with cRGD peptides for magnetic resonance imaging of brain tumors.* Biochimica et Biophysica Acta (BBA) - General Subjects, 2016. DOI: 10.1016/j.bbagen.2016.12.020.
217. Kitagawa, T., et al., *RGD targeting of human ferritin iron oxide nanoparticles enhances in vivo MRI of vascular inflammation and angiogenesis in experimental carotid disease and abdominal aortic aneurysm.* Journal of Magnetic Resonance Imaging, 2016.DOI: 10.1002/jmri.25459.
218. Wang, J., et al., *MR/SPECT Imaging Guided Photothermal Therapy of Tumor-Targeting Fe@Fe3O4 Nanoparticles in Vivo with Low Mononuclear Phagocyte Uptake.* ACS Applied Materials & Interfaces, 2016. **8**(31): p. 19872-19882.
219. Huang, R., et al., *High Precision Imaging of Microscopic Spread of Glioblastoma with a Targeted Ultrasensitive SERRS Molecular Imaging Probe.* Theranostics, 2016. **6**(8): p. 1075-1084.
220. Yang, Y., et al., *Tumor Angiogenesis Targeted Radiosensitization Therapy Using Gold Nanoprobes Guided by MRI/SPECT Imaging.* ACS Applied Materials & Interfaces, 2016. **8**(3): p. 1718-1732.
221. Zhang, L., et al., *A Multifunctional Platform for Tumor Angiogenesis-Targeted Chemo-Thermal Therapy Using Polydopamine-Coated Gold Nanorods.* ACS Nano, 2016. **10**(11): p. 10404-10417.
222. Zeng, C., et al., *Intraoperative Identification of Liver Cancer Microfoci Using a Targeted Near-Infrared Fluorescent Probe for Imaging-Guided Surgery.* Scientific Reports, 2016. **6**: p. 21959.
223. Chen, W.-H., et al., *Rational design of multifunctional magnetic mesoporous silica nanoparticle for tumor-targeted magnetic resonance imaging and precise therapy.* Biomaterials, 2016. **76**: p. 87-101.
224. Gao, W., et al., *Photodynamic Therapy Induced Enhancement of Tumor Vasculature Permeability Using an Upconversion Nanoconstruct for Improved Intratumoral Nanoparticle Delivery in Deep Tissues.* Theranostics, 2016. **6**(8): p. 1131-1144.
225. Rahman, S., et al., *The integrin alpha IIb beta 3 contains distinct and interacting binding sites for snake-venom RGD (Arg-Gly-Asp) proteins. Evidence that the receptor-binding characteristics of snake-venom RGD proteins are related to the amino acid environment flanking the sequence RGD.* Biochem J, 1995. **312 (Pt 1)**: p. 223-32.
226. Bradbury, M.S., et al., *Clinically-translated silica nanoparticles as dual-modality cancer-targeted probes for image-guided surgery and interventions.* Integrative Biology, 2013. **5**(1): p. 74-86.

227. An, T. et al. *Exosomes serve as tumour markers for personalized diagnostics owing to their important role in cancer metastasis.* J. Extracellular Vesicles 2015, 4: p.27522-27538.

228. Schwaiger, M. *PET/MR as tool for 'precision medicine'* Cancer Imaging 2014, 14(Suppl 1):O34

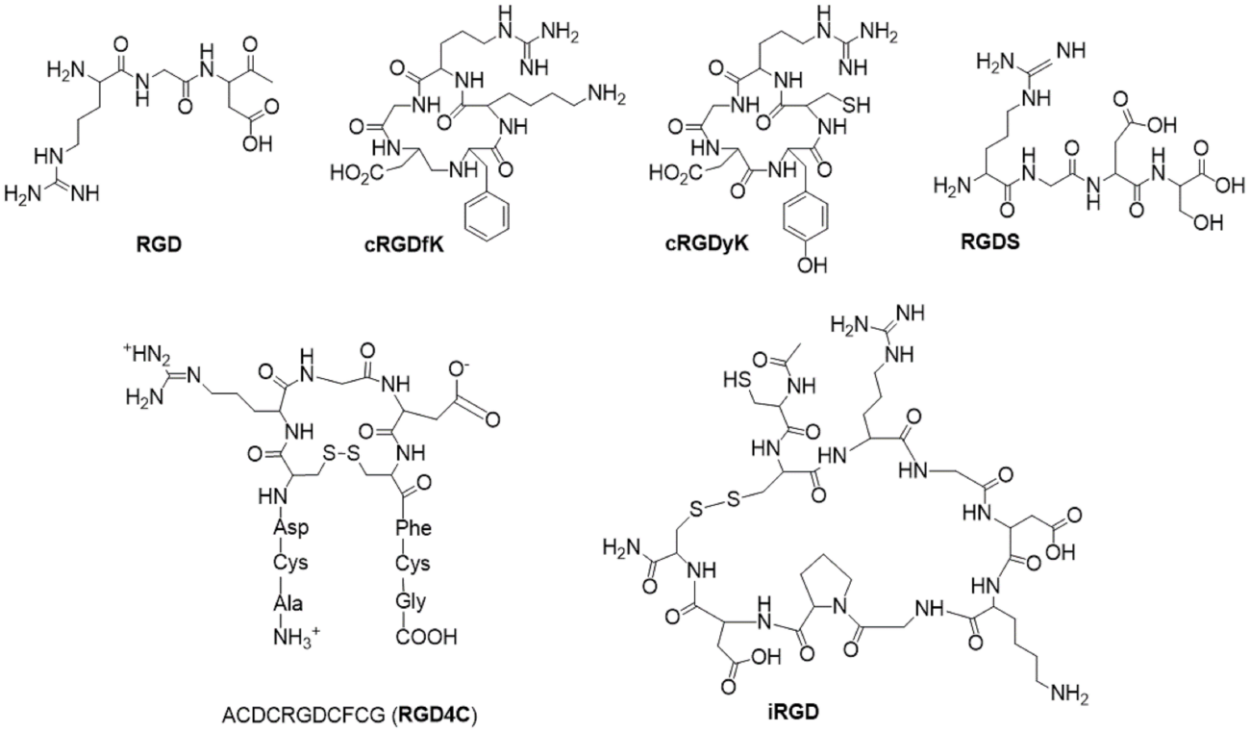

Figure 1

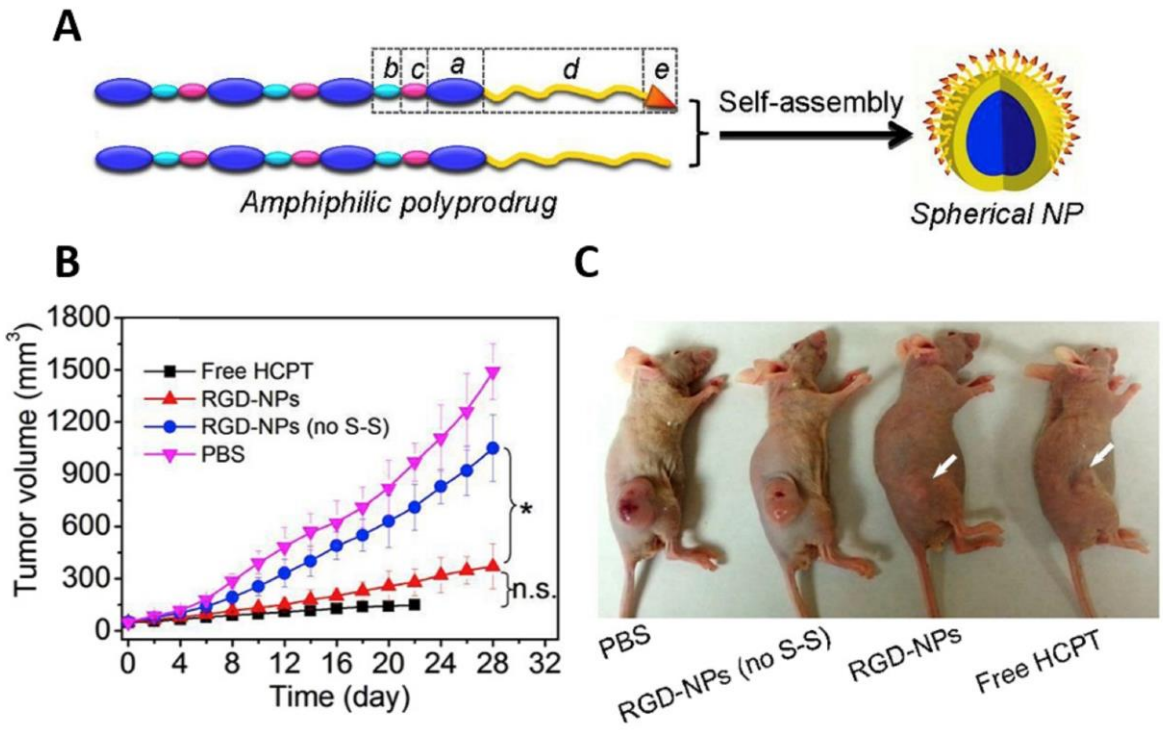

Figure 2

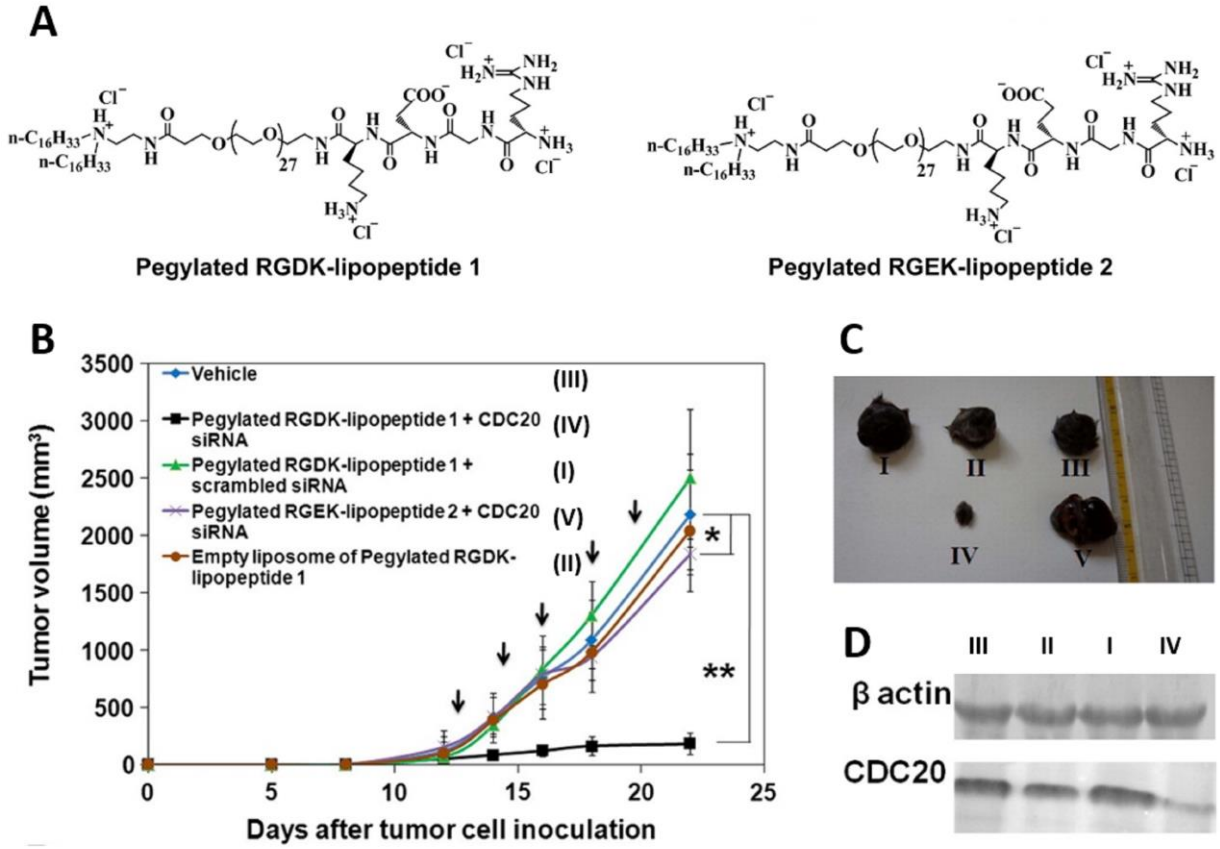

Figure 3

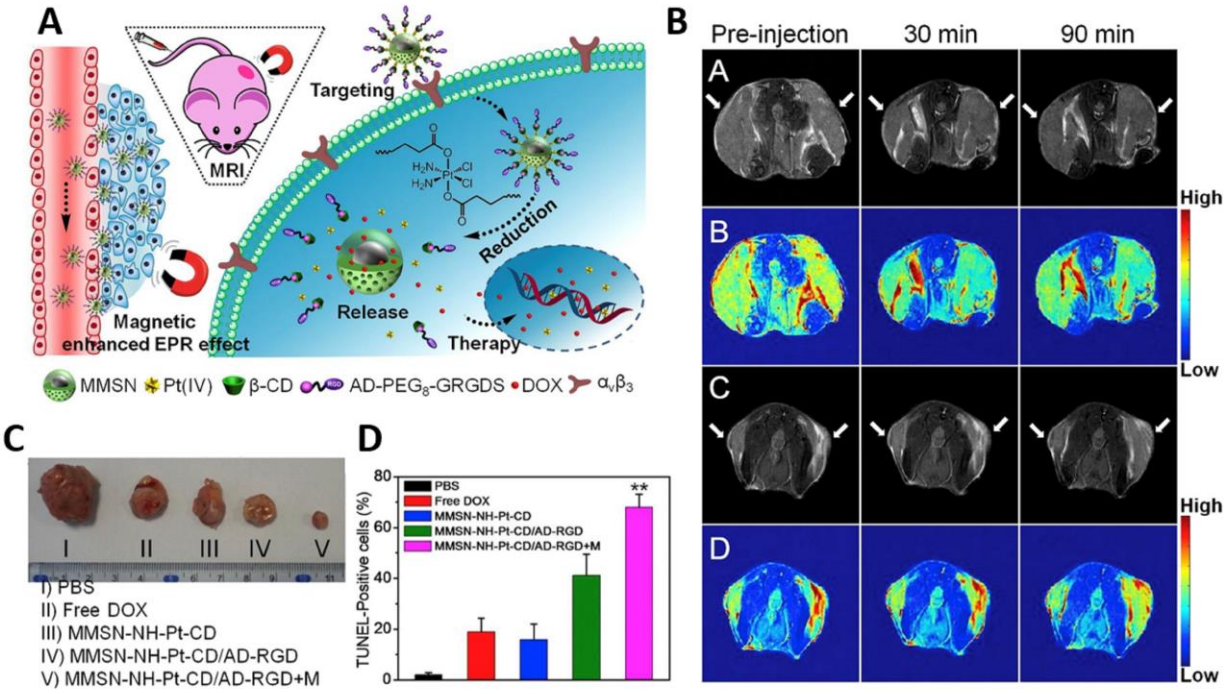

Figure 4